Biomass and Bioenergy 207 (2026) 108706

Contents lists available at ScienceDirect

Biomass and Bioenergy

journal homepage: www.elsevier.com/locate/biombioe

Application of organic geochemistry to the characterization of hydrochar and biochar: Insights into composition and optimization

Michael A. Kruge [a], Teresa A. Centeno [b], Álvaro Amado-Fierro [b], José Manuel González-LaFuente [c], Rubén Forján [d,e], José Luis R. Gallego [d,*]

[a] Earth & Environmental Studies Dept., Montclair State University, 1 Normal Ave., Montclair, NJ, 07043, USA
[b] Carbon Science and Technology Institute (INCAR-CSIC), Francisco Pintado Fe 26, 33011, Oviedo, Spain
[c] R&D, COGERSA SAU, Carretera de Cogersa 1125, 33697, Gijón, Spain
[d] INDUROT and Environmental Biogeochemistry & Raw Materials Group, Campus of Mieres, University of Oviedo, 33600, Mieres, Spain
[e] GEAPAGE Group, Department of Soil Sciences, Faculty of Agricultural and Environmental Sciences, University of Salamanca, 37007 Salamanca, Spain

ARTICLE INFO

Keywords:
Organic solid waste
Hydrothermal carbonization (HTC)
Hydrochar
HAWK® pyrolysis-FID/IRD
Pyrolysis-GC-MS
Carbonaceous material optimization

ABSTRACT

Hydrothermal carbonization has garnered significant attention in recent studies due to potential applications of the hydrochar produced, which overlap with those of torrefied biochar, including soil improvement, carbon sequestration, and energy production. However, unlike the relatively uniform properties of biochar, hydrochar characteristics can vary greatly depending on the feedstock used. Advanced characterization techniques are essential to better understand these materials and enhance their practical applications. Research on hydrochar requires a multi-faceted approach, including molecular-level studies, to optimize production processes and identify specific applications.

In this regard, analytical methods commonly used in organic geochemistry could play a crucial role in deepening our knowledge of hydrochar and biochar. Thus, this study evaluates the properties and key characteristics of five types of hydrochar and a reference biochar using a range of advanced analytical techniques. Among these, HAWK® pyrolysis with flame ionization and infra-red detectors (Py-FID/IRD) — typically employed in petroleum geochemistry — has proven to be a rapid and effective method for assessing some key properties and facilitating quick comparisons. Additionally, thermal desorption and pyrolysis analysis followed by gas chromatography coupled with mass spectrometry (TD-Py-GC-MS) provided detailed molecular characterizations of the hydrochars. These findings demonstrate that traditional techniques used in fossil fuel and environmental geochemistry are equally applicable in this field. Consequently, these techniques offer valuable insights into hydrochar composition, addressing critical knowledge gaps and leveraging advanced geochemical methods to assist in optimizing carbonaceous materials for practical applications including production of biofuels and platform chemicals for bio-refining.

1. Introduction

The issue of organic solid waste is a growing environmental concern, emphasizing the need for sustainable management to prevent pollution and resource loss. The diversity and volume of organic waste present both challenges and opportunities for recovery and circularity [1–3]. To reduce landfill dependency, innovative strategies are essential to transform organic waste into valuable byproducts for agriculture and energy applications [4]. Common solutions include composting to produce nutrient-rich soil amendments, biofuel production, and carbonization processes like torrefaction (dry pyrolysis) to create biochar [5–7]. Biochar, a carbon-rich material, has diverse applications as a pollutant adsorbent, soil amendment, biofuel, and a means for carbon sequestration [8–10]. A newer approach, hydrothermal carbonization (HTC), converts organic waste into hydrochar under high-temperature, water-based conditions, opening additional opportunities [11–17]. The properties of both biochar and hydrochar vary based on the biomass feedstock (e.g., wood vs. algae) and the carbonization method used.

The potential and importance of hydrochar applications have gained significant attention in recent literature, particularly when compared to

* Corresponding author.
E-mail address: jgallego@uniovi.es (J.L.R. Gallego).

https://doi.org/10.1016/j.biombioe.2025.108706
Received 9 September 2025; Received in revised form 19 November 2025; Accepted 20 November 2025
Available online 25 November 2025

the uses of biochar. While both materials serve as valuable byproducts for applications such as soil amendment, carbon sequestration, and energy production as a biofuel feedstock [18], and engineering applications [19], key differences arise from their production processes and properties [20,21]. Hydrochar, produced via hydrothermal carbonization, exhibits unique characteristics that vary greatly depending on the feedstock source [22], whereas biochar, derived from torrefaction or pyrolysis, tends to have more uniform properties [23]. Common techniques for characterizing these materials, such as spectroscopy, thermal analysis, and surface morphology assessments, are essential for understanding their specific properties and optimizing their applications [24–26].

A deeper investigation in the processes involved in hydrochar generation requires multifaceted studies, including on the molecular level, to optimize production, tailor applications, and be used to complement the other techniques mentioned above. In this sense, advanced analytical methods traditionally employed for fossil fuel characterization and environmental studies could play a crucial role in addressing existing knowledge gaps. For instance, HAWK® and the similar Rock-Eval® pyrolysis methods constitute a widely used analytical technique in geochemistry and petroleum exploration, primarily for evaluating the hydrocarbon potential of rock samples to assess the quality and maturity of organic material, as well as its potential to generate hydrocarbons [27,28]. We hypothesize that they could also be very useful for hydrochar characterization. Also, TD-Py-GC/MS has proven effective in analyzing complex oil compositions and resolving intricate contamination scenarios [29,30], providing valuable insights. In the context of hydrochar research, this technique could similarly contribute to a deeper understanding of the material's composition and behavior, enabling more targeted and efficient applications.

Building on these considerations, this study investigates the potential of advanced analytical techniques from organic geochemistry to examine five types of hydrochar produced via hydrothermal carbonization of organic waste streams, alongside their respective feedstocks. These hydrochars are further compared with a commercial biochar for reference. The feedstocks include scrap wood (e.g., construction waste and discarded furniture), green waste from groundskeeping, winery pomace, and the organic fraction of separately collected municipal solid waste. HAWK pyrolysis and TD-Py-GC/MS are here applied for the first time to characterize hydrochar, and, along with thermogravimetric analysis and Fourier transform infra-red spectroscopy, are employed to examine these non-traditional carbonaceous materials, providing detailed insights into their composition and potential environmental or industrial applications. Elaborating upon prior work with the same materials [31,32], the comprehensive approach presented herein aims to elucidate the key compositional and property differences between hydrochar and biochar, demonstrating the relevance and the limitations of these techniques for optimizing carbonaceous materials for practical use.

2. Materials and methods

2.1. Samples and their sources

Representative samples of the following wastes were used as raw materials for HTC trials at pilot plant scale:

- Organic fraction of municipal solid waste (OFMSW) separately collected in urban areas.
- Grape pomace from industrial wine production.
- "Green" waste from park and garden maintenance.
- Scrap wood derived from discarded furniture and construction/demolition activities, comprising a mix of softwoods, hardwoods, plywood, and fiberboard. This material typically contains various additives, including waxes, binders, varnishes, and oils, and was shredded before further processing.
- Whey from industrial cheese production.

OFMSW, green waste, and scrap wood were sampled at the Waste Treatment Centre of COGERSA, the regional public consortium for waste management in Asturias, Spain (www.cogersa.es). Grape pomace was supplied by the winery Bodegas Monasterio de Corias (Cangas del Narcea, Asturias, Spain). Whey was provided by the cheesemaker Quesería la Borbolla (www.queserialaborbolla.es), dedicated to the production of the cheese Afuega'l Pitu (Grado, Asturias, Spain). Hydrochars were identified as: H1 (waste wood + water), H2 (green waste), H3 (OFMSW), H4 (grape pomace) and H5 (waste wood + whey). For comparison, a commercial biochar (Vermichar S.L., Alcanadre, La Rioja, Spain) produced from *Quercus ilex* wood by dry torrefaction at 450 °C was also analyzed.

Despite the separation treatment systematically carried out by COGERSA to facilitate the subsequent recovery of the different wastes, non-biogenic components were detected in OFMSW, green waste and scrap wood (Fig. 1). The nature of these unwanted materials differs depending on the type of waste. Thus, in the case of scrap wood, pieces of metal and plastic were found, while stones and agricultural plastics were the more significant items in the green waste batch. The greatest percentage (5–7 wt%) of unwanted materials (plastic, glass, metal, cans, textile, cardboard, etc.) was detected in OFMSW. As far as possible (they are sometimes not easily visible), these components were removed manually prior to the HTC treatment of these wastes.

2.2. Hydrochar processing and instrumentation

The feedstocks were processed in a 2 m^3 reactor (Fig. 1) fed by the superheated steam (350 °C, 2.8 MPa) generated at the clinical waste-to-energy plant operated by the Solid Waste Management Consortium of Asturias (www.cogersa.es). The treated amount of each residue exceeded 130 kg in total (Table 1). Water (or whey where specified) was added to achieve a uniform 1:4 solid to water mass ratio. Steam was allowed to enter the reactor for 5 min while the release valve was open in order to allow all the trapped air to be released and ensure reactor is full of steam. After that, temperature was increased up to 195 °C and corresponding saturation pressure (1.3 MPa) for a period of 30 min. Once operating temperature was reached, it was maintained for 3 h, after which the release valve was opened, allowing for the reactor to decompress until atmospheric pressure was reached. All of these steps are automated through an electronic controller. Resulting products were allowed to cool down overnight before discharge of the reactor could be performed.

After processing, excess water was expelled mechanically (30 MPa) and the solids were dried in air at 35 °C (Fig. 1B). The hydrochar yield (Y) was estimated by:

$$Y_{raw}\ (\%) = (\text{mass of dry hydrochar} / \text{mass of feedstock as received}) \times 100$$

$$Y_{dry}\ (\%) = (\text{mass of dry hydrochar} / \text{mass of dry feedstock}) \times 100$$

2.3. Bulk, proximate, and ultimate analyses

Moisture and ash contents were evaluated using ASTM7582-10 in a LECO TGA701, while volatile matter (VM) was determined according to UNE-019 (ISO562). Fixed carbon (FC) percentage was estimated as 100-[VM]-[Ash]. The CHN analysis was performed following ASTM D5373 (LECO CHN-2000) and ASTM D4239 (LECO-S631) was used to evaluate the S content. The oxygen percentage was calculated as 100–[Ash]–[C]–[H]–[N]–[S]. Higher heating value determination was conducted in accordance with UNE 32006:1995 in an IKA-C4000 calorimeter.

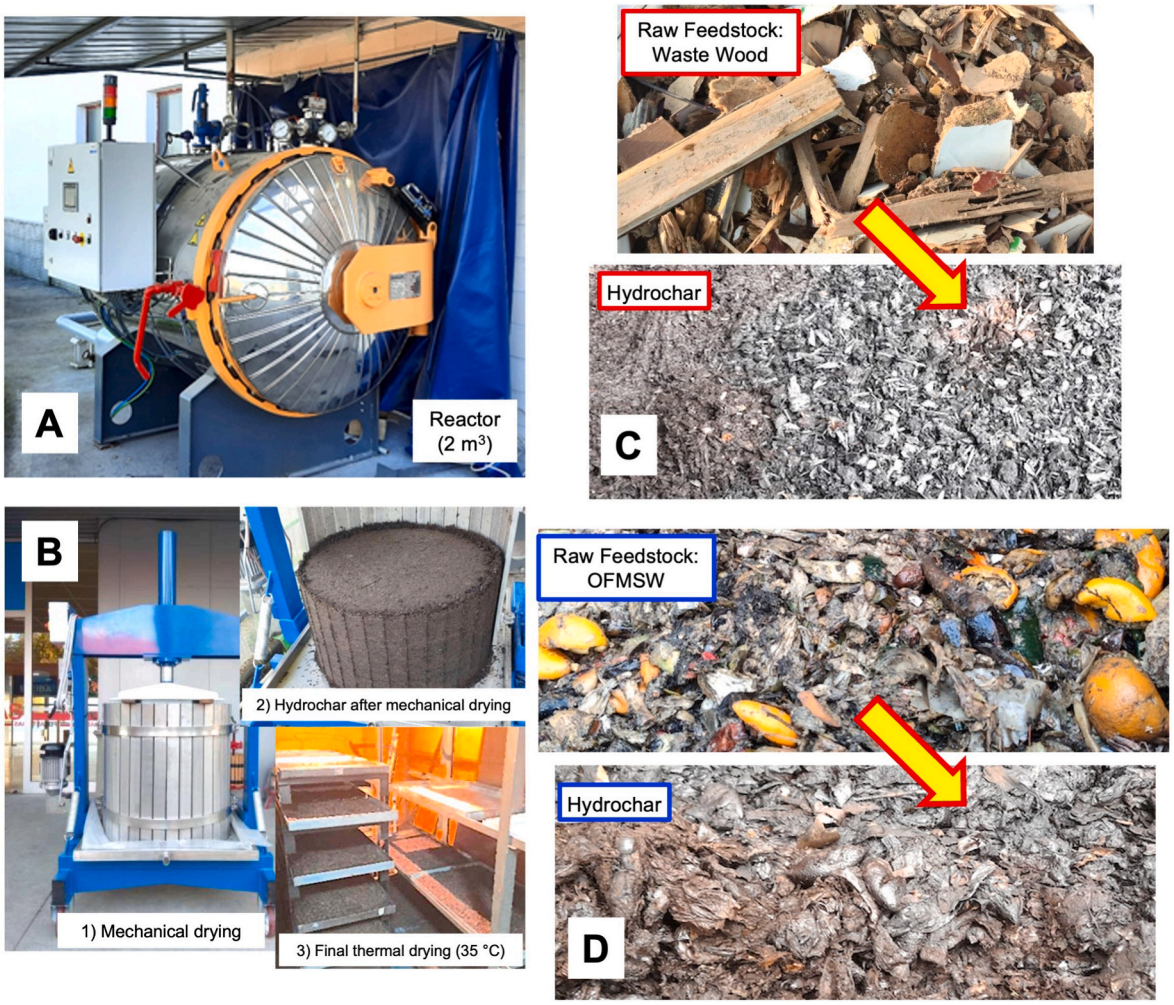

Fig. 1. A) Photograph of the hydrothermal carbonization reactor. B) Mechanical drying press, example of a hydrochar sample after pressing, and final drying procedure. C) Raw waste wood prior to processing and its resulting hydrochar. D) Raw food waste (OFMSW) and its resulting hydrochar.

2.4. Thermogravimetry (TGA)

Thermogravimetric tests were carried out in a high-capacity Mettler TGA/DSC 1 STAR thermal analysis system (Mettler–Toledo S.A.E., Barcelona) at a constant rate of 20 °C min^{-1} from 30 to 1000 °C with a holding time of 5 min in pyrolysis mode under a nitrogen atmosphere. For quality control and assurance, two hydrochars (OFMSW and green waste) were analyzed in duplicate; their mean values are employed in this article. Deconvolution was performed manually on an Excel spreadsheet, iterating the peak position, height, and width of a number of Gaussian functions until their sum closely matched the experimental data.

2.5. HAWK® pyrolysis

The HAWK® device (Wildcat Technologies, Humble (TX) USA) is a quantitative analytical pyrolysis instrument equipped with flame ionization and infra-red detectors (Py-FID/IRD), similar to Rock-Eval®. Two hydrochars (OFMSW and waste wood + water) were analyzed using the classical pyrolysis/TOC method developed for petroleum source rock analysis [33], which resembles the Rock-Eval method previously developed for the same purpose [27,28,34]. Under a stream of He carrier gas and recording data points every 0.5 s, the sample was initially held at 300 °C for 8.5 min for the evolution of the thermovaporizable fraction with the hydrocarbon-sensitive FID response designated as the S1 peak. The temperature was then increased at 25 °C min^{-1} to 650 °C with the FID response integrated as the S2 parameter, representing the pyrolyzable organic matter fraction. Simultaneously, CO_2 and CO evolved below 390 °C were separately recorded by the IRD as the S3 and S3CO parameters and above 390 °C as S3′ and S3CO'. After pyrolysis the oven was cooled and the carrier gas changed to air. The sample was heated from 150 to 770 °C at 29.5 °C min^{-1} and held there for 4 min, while the IRD recorded the combustion-derived CO_2 and CO as the S4CO2 and S4CO parameters. Total organic carbon (TOC) was computed directly by the instrument software from S1, S2, and all S3s and S4s using a standard empirical equation whereas "residual" carbon (RC) is the summed mass fraction of carbon from S4CO2 and S4CO [35]. For quality control and assurance, the wood hydrochar was analyzed five times and the OFMSW seven times, the mean values of which are used in this article. The parameters are reported on a dry, but not ash-free basis. The HAWK instrument was repeatedly calibrated using the Wildcat Technologies external standard WT4, a rock of marine origin with 6.84 ± 0.28 mg/g S2 and 2.81 ± 0.08 wt% organic carbon, as per the laboratory's routine for petroleum source rock analysis.

2.6. Fourier-transform infrared spectroscopy

Infrared spectra were obtained in a Nicolet 8700 spectrometer, equipped with a Thermo Scientific Smart Diffuse Reflectance accessory (DRIFT) and a highly sensitive liquid nitrogen-cooled MCT-A detector. For quality control and assurance, at least 2 spectra were collected for each sample of hydrochar and biochar by capturing 64 scans with a

Table 1
Hydrochar data summary.

Bulk yields of the hydrothermal carbonization (HTC) process					
	Waste wood	*Waste wood*	*Green waste*	*OFMSW*	*Grape pomace*
	(water added)	*(whey added)*	*(from park maintenance)*	*(organic fraction of municipal solid waste)*	
Raw, as received (kg)	134	160	189	487	395
Moisture, as received (%)	13	13	25	72	56
Raw (kg, dry basis)	117	139	142	136	174
Wet hydrochar (kg)	337	318	281	216	326
Dried hydrochar (kg)	97	121	97	80	129
Hydrochar yield (%, dry basis)	83	87	68	59	74

Proximate and Ultimate Analysis (weight %, dry basis, including ash)										
	Waste wood	*Wood + water*	*Wood + whey*	*Green waste*		*OFMSW*		*Grape pomace*		*Oak biochar*
	Raw	*Hydrochar*	*Hydrochar*	*Raw*	*Hydrochar*	*Raw*	*Hydrochar*	*Raw*	*Hydrochar*	
Ash	2.6	2.6	4.9	28.7	24.3	13.3	15.4	8.5	6.2	21.1
Volatile Matter	77.5	70.9	71.2	56.0	57.5	75.9	69.2	72.7	67.9	21.1
Fixed C	19.9	26.5	23.9	15.3	18.2	10.8	15.4	18.8	25.9	57.8
C	48.8	53.0	51.9	36.6	43.7	44.2	49.8	49.6	58.3	65.7
H	5.4	5.6	5.5	4.3	4.6	6.2	6.1	5.8	5.9	2.2
N	3.2	2.5	2.1	1.7	1.2	2.6	2.7	2.1	2.5	0.7
S	0.1	0.1	0.1	0.2	0.1	0.2	0.2	0.2	0.2	0.3
O	39.9	36.2	35.5	28.5	26.1	33.5	25.8	33.8	26.9	10.0
H/C molar	1.33	1.26	1.27	1.41	1.26	1.68	1.47	1.40	1.21	0.40
O/C molar	0.61	0.51	0.51	0.58	0.45	0.57	0.39	0.51	0.35	0.11
Higher Heating Value (HHV, MJ/kg)	19.7	21.7	20.4	14.3	17.5	18.9	21.4	19.0	24.0	21.1
Energy densification ratio		1.10	1.04		1.22		1.13		1.26	
Energy yield (%)		91.7	90.0		83.7		66.5		93.8	

Thermogravimetry summary. Cumulative mass loss (%) by indicated temperature.										
Temperature (°C)	*Waste wood*	*Wood + water*	*Wood + whey*	*Green waste*		*OFMSW*		*Grape pomace*		*Oak biochar*
	Raw	*Hydrochar*	*Hydrochar*	*Raw*	*Hydrochar*[a]	*Raw*	*Hydrochar*[a]	*Raw*	*Hydrochar*	
300	19.5	11.8	16.1	15.0	11.2	28.9	20.7	27.1	18.6	3.8
350	42.2	28.3	40.6	29.3	24.4	51.3	40.4	43.1	24.0	4.7
400	68.8	59.1	57.3	38.2	43.1	60.3	51.2	51.1	45.8	5.6
600	77.3	70.3	67.8	47.7	55.4	70.7	63.8	66.6	63.2	10.1
1000 (end of run)	86.1	80.2	75.1	58.9	68.1	80.0	73.6	76.0	71.7	22.0
(loss by 300 °C)/ (loss by 610 °C) (%)	25	17	24	32	20	41	32	41	29	37

[a] Mean of 2 determinations.

resolution of 4 wavenumbers (data spacing of 1.928 cm^{-1}) in the mid-infrared range (4000–650 cm^{-1}).

2.7. Thermodesorption- and pyrolysis-gas chromatography-mass spectrometry

The "double-shot" TD-Py-GC-MS (thermodesorption and sequential pyrolysis-gas chromatography-mass spectrometry) procedure was applied to obtain the molecular fingerprint of the five hydrochars and the biochar used in this study. In brief, it consisted of a two-step analysis in which an initial thermodesorption (TD) was performed at lower temperatures, and the remaining sample residue was subsequently heated at a higher temperature to evolve the true pyrolysis products [29, 30]. "Single-shot" Py-GC-MS, in which the sample is analyzed only once at the higher temperature, was also used in an experiment with two of the hydrochars.

TD-Py-GC-MS were accomplished using a PY-2020iD double-shot pyrolyzer (Frontier Lab, Japan) coupled to a GCMS-QP2010 Plus (Shimadzu Europe, Germany) equipped with an Agilent DB-5ms capillary column (5 % phenyl, 95 % dimethylpolysiloxane; 60 m × 0.25 mm i.d. x 0.1 μm film) with He as the carrier gas. Thermodesorption was performed on 1 mg samples for 20 s at 350 °C. The oven temperature of the GC was programmed from 50 to 310 °C (at 2.5 °C min^{-1}), with an initial hold of 2 min at 50 °C and a final hold of 45 min at 310 °C. The mass spectrometer was operated in EI mode at 70 eV, calibrated daily by autotuning with PFTBA, and operated in full-scan mode (50–600 *m/z*). After the TD run had ended, the sample (which had remained untouched in the pyrolyzer) was heated at 610 °C for 20 s, thereby pyrolyzing the post-thermodesorption residue ("double-shot" or "sequential pyrolysis"). Pyrolysis products were analyzed by GC-MS using the conditions employed for the TD products. In cases for which the initial amount was inadequate for optimal signal-to-noise or excessive, leading to column overloading, the sample quantity was adjusted and the analysis repeated. For "single-shot" Py-GC-MS, the sample was heated only once, at 610 °C for 20 s, followed by GC-MS analysis using the above conditions. Compounds were identified using the W8N08 (John Wiley & Sons, Inc., New York), NIST27, and NIST47 (chemdata.nist.gov) mass spectral libraries, the online NIST Standard Reference Database Number 69 (webbook.nist.gov/chemistry/), and by reference to the literature, as specified in Section 3.

3. Results

3.1. Process yields and bulk analyses

Operating the hydrothermal carbonization experiments at pilot plant

scale (Fig. 1A) required appropriately large amounts of feedstock at the outset: 134–487 kg of raw waste (Table 1). Drier material, such as the wood waste (only 13 % moisture), required the addition of process liquid, while the wetter did not — the OFMSW (72 % moisture) was sufficiently wet as received. A notable feature of hydrothermal carbonization (essentially hydrous pyrolysis) is that it avoids the energy-intensive pre-drying of the feedstock, as water is obviously essential to the process.

After mechanical and thermal drying, the resulting hydrochars were gray-colored and of similar mass (80–129 kg) (Table 1, Fig. 1B–D). In a separate experiment, wood waste was processed with caseiculture whey (94 % moisture) instead of tap water in order to simultaneously valorize two waste streams. This yielded proportionately about the same amount of dry hydrochar as the wood processed with water. The other materials, particularly the OFMSW, yielded significantly less (Table 1). Analysis of the process liquids after HTC was beyond the scope of this project.

3.1.1. Proximate and ultimate analyses

The ash contents of the raw feedstock vary considerably, from 3 % for the wood waste to 31 % of the green waste. The latter, being groundskeeping trimmings, likely includes some soil material which escaped removal during preliminary visual inspection (Sec. 2.1). In general, the hydrochars tend to exhibit slightly less volatile matter, but marginally more fixed carbon than the raw feedstocks (Table 1).

The molar H/C and O/C ratios exhibit a parallel decrease during hydrothermal carbonization, from compositions consistent with biomass to those compatible with peat and lignite (Table 1, Fig. 2). Nitrogen contents are low, ranging from 1.2 % in the green waste hydrochar to 2.7 % in that of the OFMSW. Sulfur concentrations (≤0.3 %) are negligible. The mean higher heating value of the hydrochars is 21 MJ kg^{-1}, a modest increase from the mean for the raw materials (18 MJ kg^{-1}, Table 1). These values tend to decrease with increasing ash content and are comparable to low rank coal (15–33 MJ kg^{-1} [36]). Amado-Fierro et al. [31] presented the proximate and ultimate analysis results in greater detail.

Hydrothermal treatment resulted in energy densification across all feedstocks, confirming that the process effectively concentrates the energy content of the raw materials. This densification appears to be influenced by the initial moisture content of the feedstock, as hydrochars derived from waste wood exhibited lower energy densification ratios than those produced from wetter materials such as green waste or OFMSW. Conversely, the drier feedstocks achieved higher solid yields, which partially compensated for their lower densification and enhanced their overall energy recovery potential. The highest energy yields were observed for waste wood and grape pomace, suggesting that factors other than moisture content also play a significant role in determining the overall energy performance.

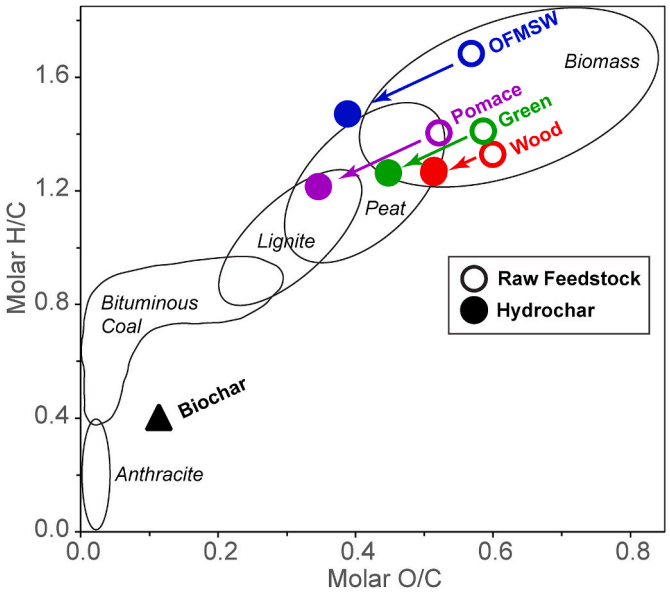

Fig. 2. Van Krevelen diagram showing transformations resulting from the conversion of biomass to hydrochar, as well as oak biochar for comparison, after Amado-Fierro et al. [31]. Interpretive fields after Koppejan and van Loo [82]. Note that the two waste wood hydrochars have nearly the same coordinates (Table 1) and plot superimposed.

In contrast to the hydrochars, the oak biochar sample exhibits much lower volatile matter and higher fixed carbon contents, along with very low molar H/C and O/C ratios, comparable to those of high-rank coal (Table 1, Fig. 2).

3.2. Thermogravimetric analysis

All five hydrochar samples exhibit a rapid phase of decomposition between approximately 350 and 400 °C during thermogravimetric analysis (TGA) in pyrolysis mode, above which temperature there is only gradual further breakdown (Fig. 3A). Overall, the hydrochars lose roughly half of their mass by 400 °C, losing about 75 % by the end of the process at 1000 °C (Table 1). The two waste wood hydrochars have the sharpest transformation, while that of the green waste appears more gradual, although this may be due to the latter sample's higher ash content. (Fig. 3A–Table 1).

3.2.1. First derivative thermogravimetric analysis

Viewing the first derivative of the thermogravimetric traces (DTG) of the waste wood, the inflection points marking the temperature of the maximum rate of conversion (T_{max}) are nearly the same for the raw feedstock and the hydrochar processed with water (ca. 370 °C, Table 1, Fig. 3B). The principal difference between these two results is that the raw wood begins major decomposition about 50 °C lower, producing a broader peak. Interestingly, the wood hydrochar processed with whey exhibits a narrow peak, similar to the water-based hydrochar, but shifted down by ca. 20 °C. Note that all the thermograms exhibit a minor peak maximizing at about 60 °C, likely due to the loss of residual moisture (Fig. 3B–F).

The raw green waste, with a T_{max} of 350 °C, shows a bulging initial shoulder and a broad post-peak tail extending out to ca. 500 °C, with a minor final peak centered on 660 °C (Fig. 3C). The principal peak of its hydrochar is sharper, maximizing at the slightly higher temperature of 370 °C, but with a similar post-peak tail and minor feature at 660 °C.

The complex thermograms of the organic fraction of municipal solid waste (OFMSW) display multiple features. Its hydrochar, with a T_{max} of 340 °C, has auxiliary inflection points at 250, 390, 480, and 680 °C (Fig. 3D). The raw feedstock behaved similarly upon heating, but as with wood and green waste, began intense decomposition at a lower temperature.

The thermograms of raw grape pomace and its hydrochar show striking differences. The feedstock has two sharp low temperature peaks at 285 and 305 °C followed by a broad plateau with secondary maxima at about 345 and 450 °C (Fig. 3E). Its hydrochar exhibits a broad zone of heterogenous decomposition between 200 and 500 °C, with maxima at 275 and 350 °C, in near alignment with the feedstock.

As evidenced in Fig. 3A and Table 1, the oak biochar is principally refractory OM, yielding little upon pyrolysis. Its DTG curve, maximizing at the high temperature of 685 °C, is otherwise nearly featureless (Fig. 3F), standing in sharp contrast with the hydrochars. We note that the heterogenous green waste and OFMSW produced small, high-temperature peaks (660–680 °C), likely indicating a minor char component (Fig. 3C and D).

3.2.2. Deconvolution of TGA results

The complexity of the DTG curves implies the presence of multiple components with differing thermal properties, unsurprising given that

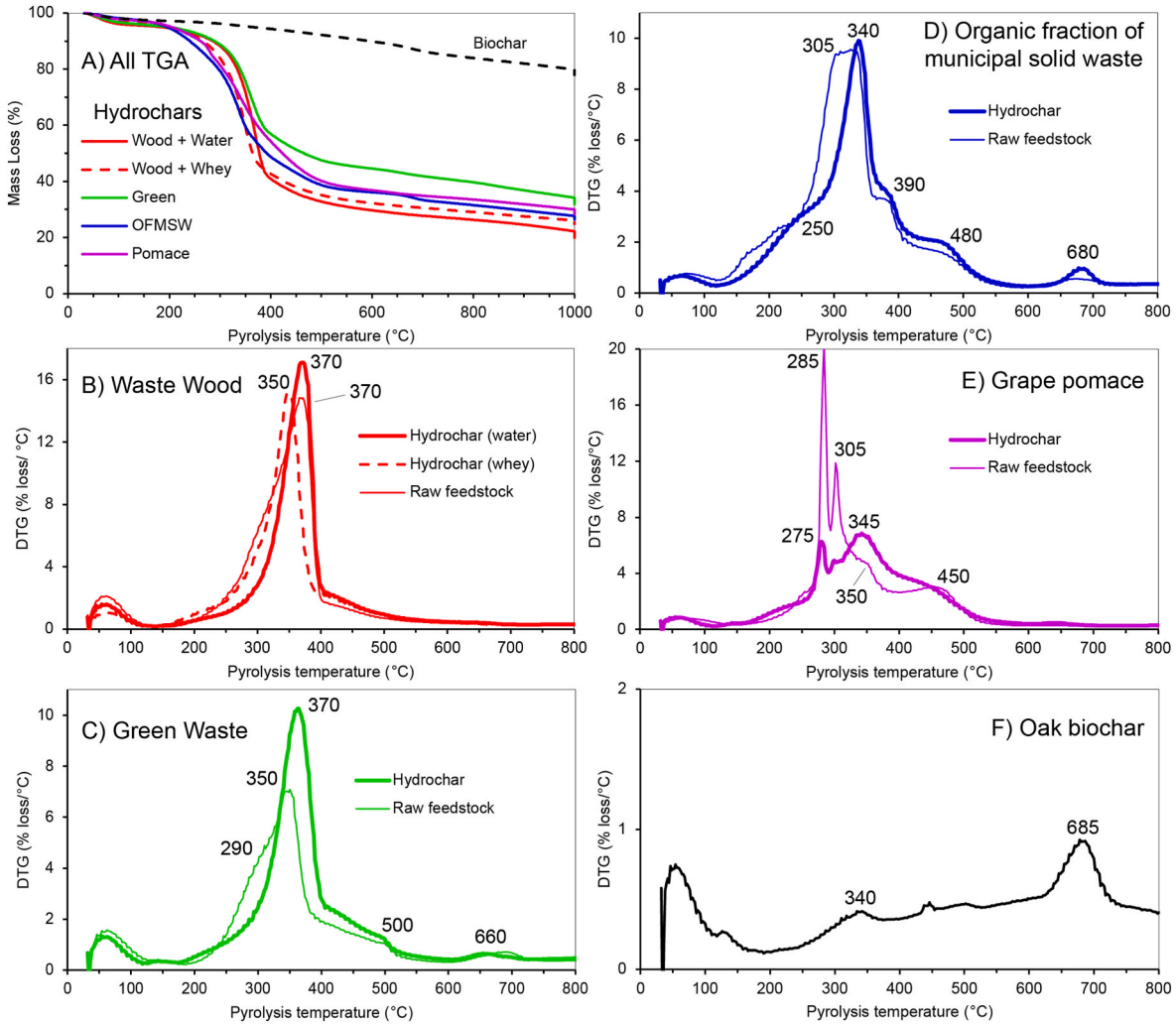

Fig. 3. A) TGA thermograms showing mass loss as a function of temperature for the five hydrochar samples and oak biochar. B) DTG traces for waste wood feedstock and hydrochars. C) DTG traces for park maintenance green waste feedstock and hydrochar. D) DTG traces for the OFMSW feedstock and hydrochar. E) DTG traces for grape pomace feedstock and hydrochar. F) DTG trace for oak biochar. Temperatures of principal inflections points are posted.

the materials are heterogenous wastes. The OM likely includes fats, cellulose, hemicellulose, lignin, and char. To further investigate this heterogeneity, we deconvoluted the DTG traces of the feedstock and hydrochars of two samples (waste wood with water and OFMSW) for which the bulk and TGA data indicate significant differences (Secs. 3.1, 3.2.1).

Previous TGA work studying the thermal behavior of biomass emphasized hemicellulose, cellulose, and lignin as the most relevant plant biopolymers. Proposed kinetic parameters showed considerable variation, due to the use of different taxa and experimental conditions [22,37–40]. The literature consensus is that hemicellulose is the most labile of the three and that lignin exhibits a broad activation energy range, in part taxon-dependent.

In the present case, application of this three-component deconvolution model to the hydrochars and their feedstocks produced only rough matches to the experimental data, worse in the case of OFMSW. Rather, the irregularities in the raw OFMSW thermogram (Fig. 3D and 4A) readily suggest peak temperatures for various deconvolution pseudo-components. After experimenting with several configurations, the best results were achieved with seven pseudo-components of differing breadth and intensity, with peak temperatures ranging from 245 to 680 °C (Fig. 4A). The resulting model (dashed curve summing the 7 individual peaks) closely tracks the DTG data (heavy black line). While we make no claim that this result is a unique solution, it matches the experimental data quite well. No attempt was made to model the minor features on the extreme ends of the DTG curves (<100 and >750 °C).

These same seven pseudo-components (i.e., having identical peak temperatures) were then employed to deconvolute the DTG trace of the OFMSW hydrochar, iteratively adjusting peak height and width until a satisfactory match was achieved (Fig. 4B). This successful result serves to further validate the initial choice of the seven peak temperatures, which – being the same – more readily permit a comparison between feedstock and hydrochar. It is evident that the most profound effect of the hydrothermal conversion is the marked reduction in the two low temperature pseudo-components (245 and 305 °C). The distribution of the five higher temperature peaks remains relatively intact, with a narrow 336 °C pseudo-component as the most prominent for the hydrochar.

In contrast to the OFMSW, the DTG of the waste wood and its hydrochar trace single, massive central peaks without major irregularities (Fig. 3B). Nevertheless, the raw wood feedstock data responded well to deconvolution using seven pseudo-components. Initially, the peak temperatures employed were the same as those used for the OFMSW. After several iterations, a better model was achieved by slightly adjusting most of the temperatures, in addition to varying peak width and height (Fig. 4A and D). The wood hydrochar DTG was deconvoluted with the same seven pseudo-components used for its feedstock, but necessitated a magnitude reduction of the three lowest temperature

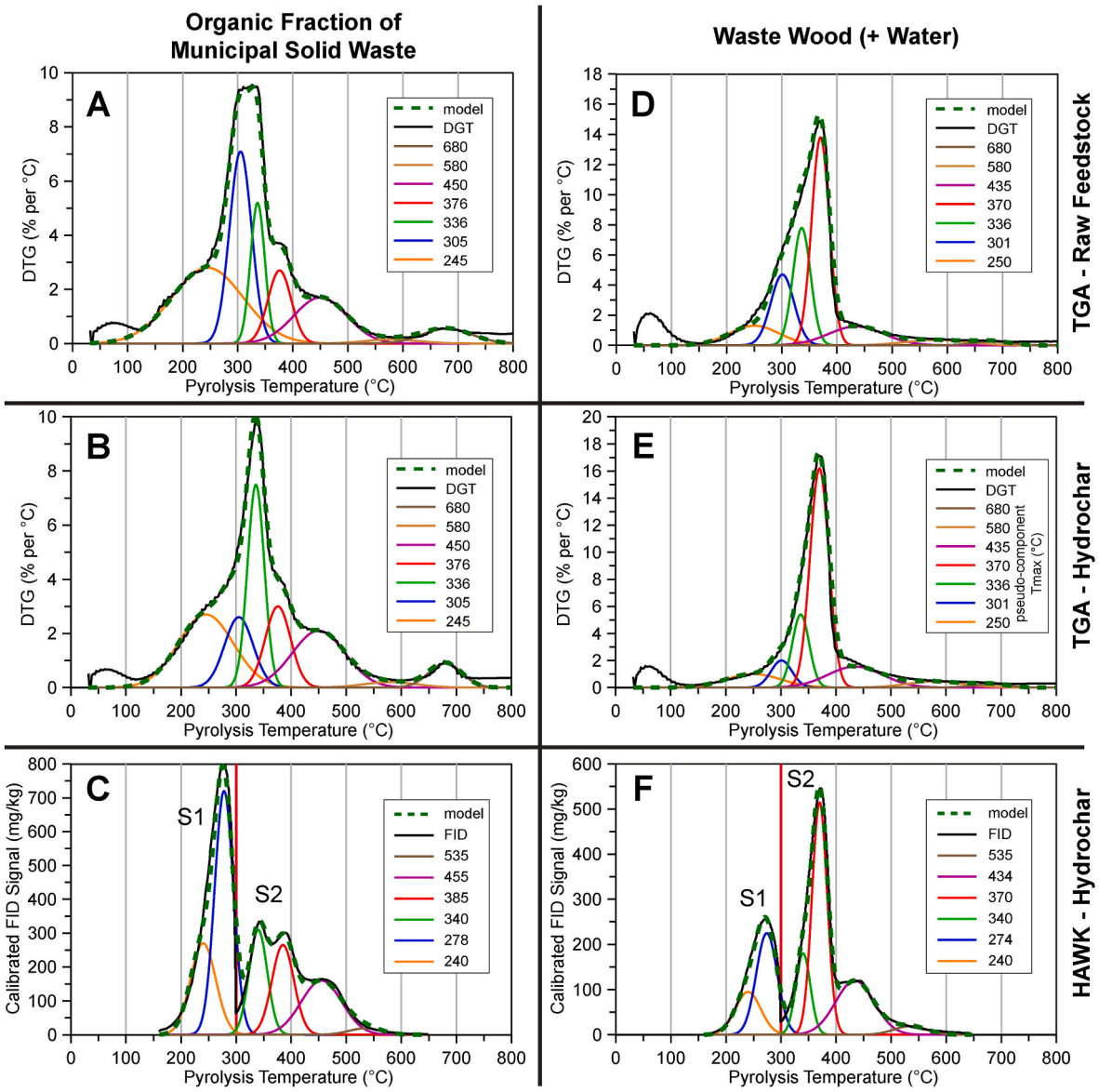

Fig. 4. Deconvoluted TGA thermograms and HAWK FID pyrograms for the wood and food waste samples. For TGA, the first derivatives (DTG, percent mass loss per °C) are plotted as a function of pyrolysis temperature. The HAWK FID signal is calibrated as mg hydrocarbons per kg sample, plotted by pyrolysis temperature. The color-coded numbers in the chart legends are the peak temperature values (T_{max}, °C) of the individual pseudo-components used in the deconvolution. A) Raw food waste (OFMSW) TGA. B) Food waste hydrochar TGA (mean of two determinations). C) HAWK FID pyrogram of food waste hydrochar (mean of seven repetitions). D) Raw waste wood TGA. E) Waste wood + water hydrochar TGA. F) HAWK FID pyrogram of waste wood + water hydrochar (mean of five repeat analyses). See Sec. 2.5 and Table 2 for definitions of S1 and S2.

features, leaving a sharp central peak at 370 °C clearly preeminent (Fig. 4E).

Although a middle temperature pseudo-component dominates both hydrochar models (336 and 370 °C respectively, Fig. 4B and E), the deconvolution exercise indicates that the OFMSW hydrochar has a greater compositional complexity, logically reflective of the highly diverse organic waste stream. With such diversity, it may be better to consider the so-called pseudo-components as simply represent groupings of coincident bond scissions in different materials as their respective activation energy thresholds are reached in parallel during heating. Fragmentation of the most labile biopolymers clearly occurs during HTC leaving the more resistant in the hydrochar (Fig. 4). This is somewhat analogous to the kinetic models that petroleum geochemists conceived for kerogen maturation [41,42], extended by Sebag et al. [43] for application to soil organic matter.

3.3. *HAWK® pyrolysis*

The HAWK® device is a Py-FID/IRD instrument that operates in a manner similar to the Rock-Eval® system, with its standard analytical results encoded in a nearly identical fashion (Sec. 2.5, Table 2). Like Rock-Eval, the HAWK method is intended primarily for petroleum source rock evaluation [28]. Nonetheless, Py-FID/IRD is increasingly finding applications in studies of recent organic matter, environmental pollution, and biofuels [43–53].

Two contrasting hydrochars (waste wood with water and OFMSW) were chosen for HAWK analysis on an experimental basis. Two of the most commonly employed petroleum source rock parameters – S1 (thermovaporizable organic fraction) and S2 (pyrolyzable fraction) – in combination demonstrate a profound difference between the two samples. While S2 is similar (209 mg pyrolyzate g^{-1} sample for OFMSW and 179 mg g^{-1} for wood), S1 for OFMSW is 83 mg thermovaporized OM g^{-1}

Table 2
HAWK pyrolysis results.

	Waste Wood		OFMSW	
	Hydrochar		Hydrochar	
	mean of 5	st. dev.	mean of 7	st. dev.
S1 Thermovaporizable Fraction (mg HC/g sample)	29	1	83	10
S2 Pyrolyzable Fraction (mg HC/g sample)	179	17	209	10
S3 (mg CO2/g sample by pyrolysis ≤390 °C)	7	0.2	6	0.7
S3' (mg CO2/g sample by pyrolysis >390 °C)	3	0.8	4	1.0
S3CO (mg CO/g sample by pyrolysis ≤390 °C)	8	0.4	5	0.5
S3′CO (mg CO/g sample by pyrolysis >390 °C)	5	0.3	2	0.5
S4CO2 (mg CO2/g sample by combustion)	747	39	486	28
S4CO (mg CO/g sample by combustion)	50	10	15	3
TOC (Total Organic Carbon) (wt. %)	40.9	1.4	39.9	1.5
RC (residual carbon by combustion) (wt. %)	22.5	0.79	13.9	0.86
PI Production Index (S1/(S1+S2))	0.15	0.01	0.30	0.03
OSI Oil Saturation Index (S1/TOC x 100)	83	9	229	27
HI Hydrogen Index (S2/TOC x 100) mg HC/g TOC	466	57	523	16
OI Oxygen Index (S3/TOC x 100) mg CO2/g TOC	18	2	16	2
CO2/(CO + CO2) pyrolysis (from S3's)	0.43	0.02	0.60	0.03
CO2/(CO + CO2) combustion (from S4's)	0.94	0.01	0.97	0.00

sample, nearly three times the 29 mg g^{-1} detected for the wood hydrochar (Table 2). Classical petroleum geochemistry parameters – Production Index and Oil Saturation Index, which are ratios emphasizing S1 – are considerably higher for OFMSW than for wood (Table 2). For both OFMSW and waste wood, total organic carbon (TOC) values are similarly high (40 and 41 %, respectively), to be expected for biomass with minimal mineral matter, as are the Hydrogen Indices (523 and 466 mg pyrolyzate g^{-1} TOC, respectively).

Since the HAWK infrared detector discriminates between pyrolytic CO and CO_2, separate S3 parameters are reported for each gas (Sec. 2.5). These are routinely subdivided at the 390 °C mark, to isolate the effect of high temperature calcination of mineral carbonate that may be present in geological samples. Although some mollusk shells are in the food waste (Fig. 1D), this effect is likely to be minor in the present case. While S3 values are similarly low for both samples (3–7 mg CO_2 g^{-1} sample), wood S3CO is nearly double that of OFMSW (Table 2). The Oxygen Indices are similarly low for both samples (16–18 mg CO_2 g^{-1} TOC), surprising since they have the relatively high molar O/C ratios of 0.4–0.5 characteristic of biomass (Table 1). This observation is based on comparisons of Py-FID/IRD and elemental analysis of source rocks and biomass [28,54,55].

3.3.1. *Py-FID/IRD pyrograms*

While classical source rock Py-FID/IRD parameters are instructive, greater insight is gained by detailed examination of the pyrograms. This is traditionally recommended in cases of petroleum source rock irregularities [28] and is increasingly used in biomass and soil studies [43,47,53,56].

FID and IRD responses are normally presented as functions of analysis time (Fig. 5A). The OFMSW S1 peak area is obviously much larger than that of the wood, consistent with the numerical values (Table 2). In the S2 region the samples display markedly different morphologies: the OFMSW hydrochar pyrogram is distinctly multi-lobed, while the wood produced a single, narrower peak followed by a broad shoulder. The combined IR pyrograms ($CO + CO_2$) show maxima tracking the principal S2 (FID) peaks, lagging behind by about a half minute, overall with

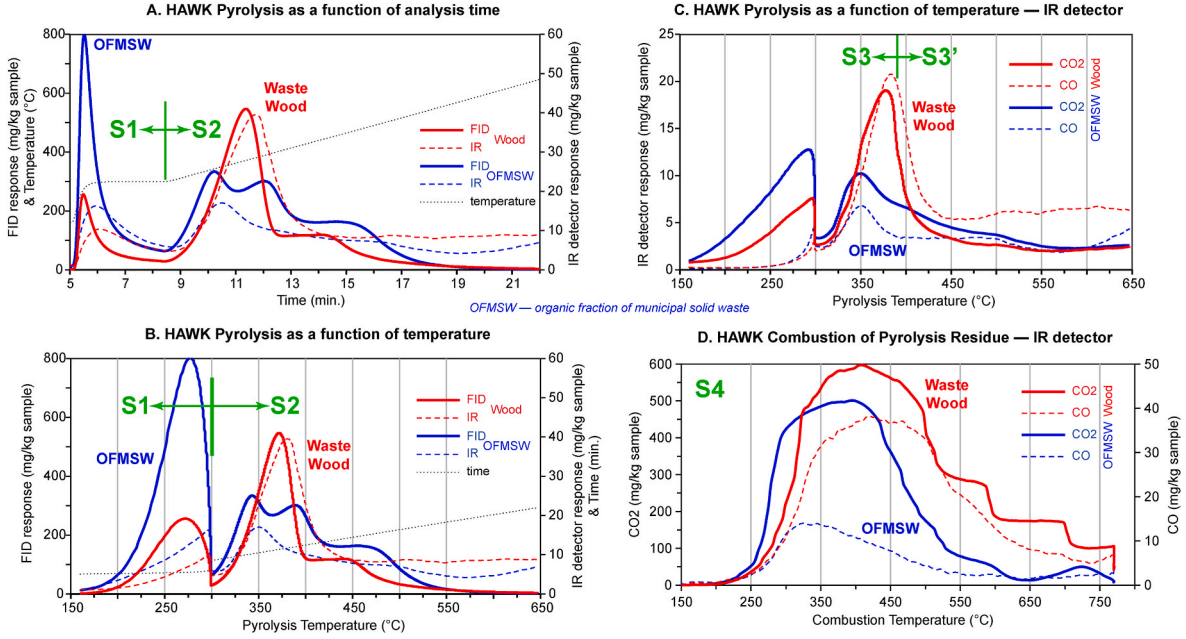

Fig. 5. HAWK pyrograms for hydrochars of the waste wood + water (in red, mean of five repeat analyses) and food waste (in blue, mean of seven repeats). A) FID and IR detector yields as a function of analysis time. B) FID and IR detector yields as a function of pyrolysis temperature. For both A and B, the FID traces (S1, S2) are shown with heavy solid lines, while the dashed lines indicate the summed IR yields for CO and CO_2 (S3 + S3CO + S3' + S3′CO). C) IR detector response as a function of temperature during pyrolysis (S3 + S3′ and S3CO + S3′CO). D) IR detector response as a function of temperature during post-pyrolysis combustion (S4 and S4CO). For both C and D, the CO_2 yields are shown with heavy solid lines, while the dashed lines indicate the CO response. See Sec. 2.5 and Table 2 for definitions of S1–S4.

greater yield at lower temperatures for the OFMSW.

3.3.2. Py-FID response viewed in the temperature domain and deconvolution

The S2 peak morphologies (Fig. 5A) recall the features of the corresponding DTG traces (Fig. 3B and D). To facilitate the comparison, the HAWK data were replotted in the temperature domain (Fig. 5B). Ignoring (for the moment) the obvious discontinuity at 300 °C marking the change from isothermal to temperature ramp, peak temperatures for the various features are clearly evident. This recognition led to an attempt at deconvolution of the Py-FID traces, beginning with pseudo-components centered on the temperature maxima in the S2 region of the OFMSW (Fig. 4C). With iterative adjustment of peak breadth and height, a well-fitting model curve began to take shape. With the tentative addition of two lower temperature peaks to model the S1 and a small higher temperature one to complete the S2 match, a satisfactory six pseudo-component model emerged. Interestingly, the peak temperatures (excluding the zone around the 300 °C discontinuity) are quite close to those employed for OFMSW TGA deconvolution, running a few degrees higher in the HAWK S2 region (Compare Fig. 4B and C). There was no seventh, high temperature pseudo-component required since Py-FID data collection ceased at 650 °C.

Beginning with the obvious 370 and 440 °C peaks on the wood hydrochar S2 curve (Fig. 5B), the addition of small lower and higher temperature peaks, and iterative adjustment, an acceptable S2 peak model was achieved (Fig. 4F). Again tentatively, two peaks under 300 °C were able to match the S1 profile. Discounting the interruption at the start of the temperature ramp, the results are comparable to TGA deconvolution of this hydrochar (Fig. 4E).

It is reassuring that for each hydrochar, the DGT and Py-FID curves could be deconvoluted by virtually the same pseudo-components above 300 °C (Fig. 4). This could be expected in that both instruments were operated in pyrolysis mode using similar heating rates (Secs. 2.4, 2.5). The hydrocarbon-sensitive FID appears to resolve the components better than the bulk mass loss recorded by the TGA. The HAWK instrument can readily be reprogrammed to employ a constant rate of increase across the full temperature range, thus avoiding the discontinuity due to the initial isothermal step. The single temperature ramp setting has already been adopted in Py-FID/IRD studies of biomass, often with deconvolution or empirically divided into temperature zones [43,44,47,48,51,53]. We conclude from our initial experiment that this should indeed be the way forward in future hydrochar characterization work.

3.3.3. Py-IRD and combustion-IRD

The ability of the IR detector to discriminate between CO and CO_2 provides an additional window into the nature of the hydrochars. Plotting the pyrolysis data for the two gases as separate curves, we note that of the two hydrochars, the waste wood yields more of both above 300 °C, but also proportionally more CO (Fig. 5C and the $CO_2/(CO + CO_2)$ S3 ratio in Table 2). The complexity of the OFMSW FID trace (Fig. 5B) is not mirrored by its simpler IRD curves. As with the FID response, the discontinuity due to the initial isothermal step interferes with observation of the initial decomposition phase, except to note that CO_2 production is greater than that of CO at the lower temperatures, particularly for OFMSW.

The post-pyrolysis residue combustion yields were on par with those from pyrolysis (Fig. 5B and D). The residual (non-pyrolyzable) carbon fraction (RC) comprises more than half of the TOC of the waste wood hydrochar, but only a third of that of the OFMSW (Table 2), values close to those determined as “fixed carbon” by proximate analysis (Table 1). Refractory components in the wood sample evidently required higher temperatures to fully react (Fig. 5D). Both hydrochars produce an order of magnitude more CO_2 than CO upon combustion ($CO_2/(CO + CO_2)$ S4 ratio in Table 2). However, as with pyrolysis, combustion of the waste wood hydrochar yielded proportionally more CO than did the OFMSW (Fig. 5C and D).

As noted for the Py-FID results, greater insight would also be obtained from the IRD with the HAWK device set to a constant pyrolysis temperature ramp without the initial 300 °C hold. The advantage of a Py-FID/IRD instrument over conventional TGA is its use of sensitive multiple detectors. Thus, it also offers an alternative to the more sophisticated TGA approaches with evolved gas analysis (e.g., TGA-FTIR, TGA-MS, TGA-GC-MS).

3.4. Fourier transform infra-red spectroscopy (FTIR)

The simple bulk and thermal analyses indicate significant differences between the hydrochars of the various feedstocks, as well as between the hydrochars and the biochar (Secs. 3.1–3.3). As the next step, FTIR spectroscopy was employed to begin the investigation of their chemical characteristics. In general, the FTIR spectra of all five hydrochars are broadly similar, with the OFMSW and pomace appearing more aliphatic; the highly aromatic oak biochar stands apart from the hydrochars [31]. Here we present a detailed examination of the FTIR spectra of the OFMSW and waste wood (with water) hydrochars, i.e., the two contrasting samples emphasized in Sections 3.2.2 and 3.3.

The spectra of both hydrochars feature a broad, prominent band at 3350 cm^{-1} assigned to O–H stretching, corresponding to the presence of carboxylic acids, alcohols, phenols and possible residual moisture (Fig. 6A). (Table 3 gives the literature sources for the band assignments and other details.) The aliphatic stretching region between 3100 and 2800 cm^{-1} provides a clear contrast between the two hydrochars. CH_2 stretching bands at 2924 and 2854 cm^{-1} are particularly sharp for the OFMSW, along with lesser, but distinct CH_3 stretching (2958 and 2872 cm^{-1}) and alkene C–H stretching (3008 cm^{-1}) bands (Fig. 6A and B). C=C alkene stretching in the OFMSW is indicated at 1653 cm^{-1}, while aliphatic C–H bending at 1464 and 1456 cm^{-1} is notable in both samples (Fig. 6C). CH_2 bending and CH scissoring are evident at 1373 cm^{-1} for both hydrochars, as is CH_2 and CH_3 scissoring (1430 cm^{-1}) associated with lignin. Aromatic C=C bands at 1605 and especially 1515 cm^{-1} are relatively more important in the wood spectrum.

C=O stretching bands at 1740 and 1705 cm^{-1} associated with carboxyl and carbonyl functions feature prominently in the OFMSW spectrum (Fig. 6C). Small but distinct amide bands at 1653 and 1541 cm^{-1} also appear here. The zone between 1400 and 1200 cm^{-1} appears similar in both spectra and is assigned to CH_2 bending, out-of-plane bending, and scissoring, O–H scissoring, and C–O stretching, associated with phenol, methoxyphenols, lignin, and cellulose. The C–O stretching bands in the 1200-1000 cm^{-1} sector are nearly alike in both spectra, and are likely due to esters, fatty acids, and polysaccharides (Fig. 6C). Minor C–C stretching bands between 800 and 900 cm^{-1} likely arise from polysaccharides in both hydrochars (Fig. 6A).

In summary, FTIR spectra of both the waste wood and OFMSW hydrochars show broad similarities. The OFMSW is distinctive in the greater preponderance of aliphatic, carbonyl, and carboxyl indicators, while the wood displays greater aromaticity, in agreement with the generalized observations of Amado-Fierro et al. [57].

3.5. Thermodesorption- and pyrolysis-GC-MS

TD-Py-GC-MS provides detailed, reproducible molecular-level analysis of solid organic matter samples, requiring only milligrams of minimally-prepared sample [58]. In recent years, it has been increasingly employed in research related to environmental fields (e.g., Refs. [29,30]). The so-called “double-shot” approach separately analyzes the thermally-desorbable (semi-)volatile organic fraction and the pyrolyzable macromolecular fraction. The thermally-desorbed products, in particular, have to been shown to correspond closely to those detected by conventional GC-MS of solvent extracts of contaminated sediments, although the latter does offer richer detail if liquid chromatographic fractions of the extract are analyzed separately [29,30]. The simpler “single-shot” Py-GC-MS approach analyzes these two fractions

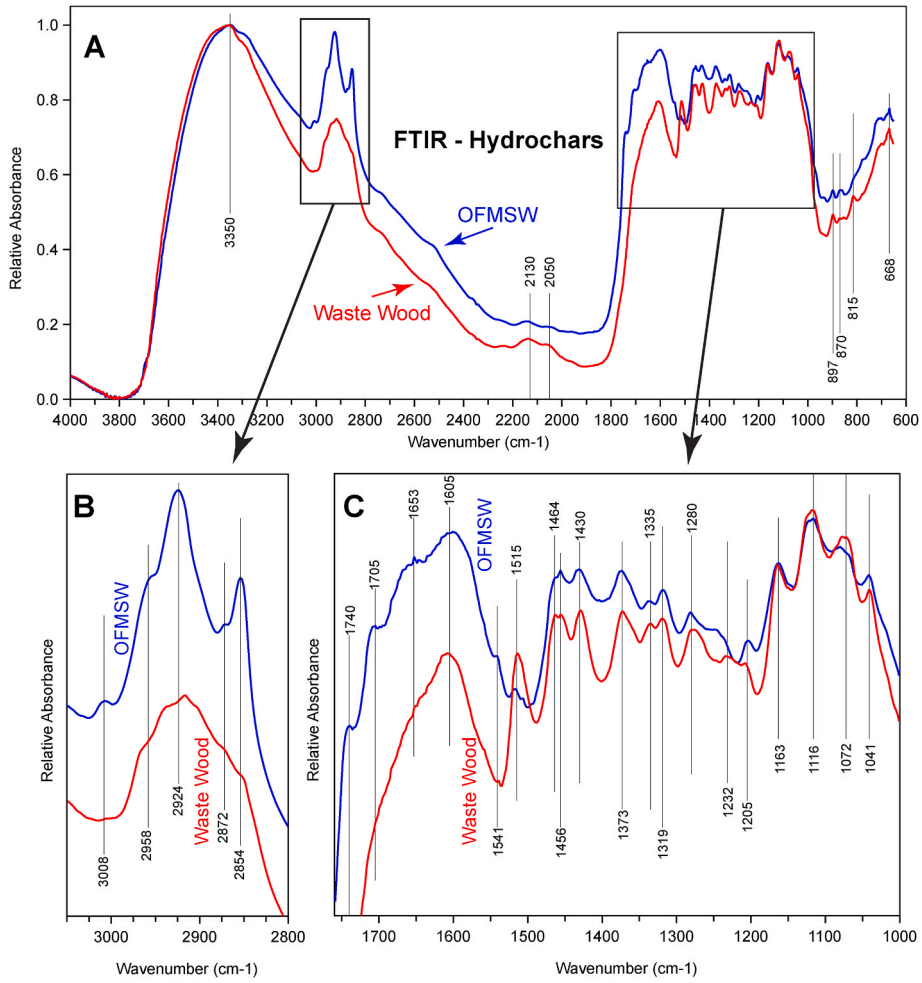

Fig. 6. Normalized FTIR absorbance spectra for hydrochars of the waste wood + water (in red, mean of 2 repeat determinations) and food waste (in blue, mean of 4 repeats). See Table 3 for band assignments. A) Full spectra. B) Detail of the 3400–2800 cm^{-1} range. C) Detail of the 1760–1000 cm^{-1} range.

combined, sacrificing some detail but saving time (Sec. 2.7).

3.5.1. *"Single-shot" Py-GC-MS of hydrochars*

The TGA, Py-FID/IRD, and FTIR results unambiguously illustrate profound differences between the hydrochars of waste wood (with water) and organic municipal waste (Sec. 3.2-3.4). Single-shot Py-GC-MS of these two hydrochars similarly reveals strongly contrasting fingerprints and additionally provides key compositional information. The wood pyrogram (Fig. 7A) displays a predominance of methoxyphenols and sugars – pyrolysis marker compounds for lignin and polysaccharides, respectively, typical of wood (e.g., Refs. [59,60]). The lignin markers are principally monomethoxyphenols, a characteristic of conifer wood pyrolyzates (e.g., Ref. [61]). The most abundant polysaccharide pyrolysis product is levoglucosan. Minor monoaromatic terpenoids also appear, likely from resins, along with long-chain *n*-alkanes ($>C_{22}$) with no odd carbon number preference, and steroids. The OFMSW hydrochar pyrogram (Fig. 7B) is radically different, primarily showing fatty acids (mostly C_{16} and C_{18}, saturated and unsaturated) and their esters, along with minor *n*-alkenes, *n*-alkanes and steroids (including cholesterol).

3.5.2. *"Double-shot" TD- and Py-GC-MS of hydrochars*

Greater detail is revealed when the hydrochars are subjected to TD-GC-MS and subsequent Py-GC-MS of the thermodesorption residue. Note that for each pair of TD and Py traces, the intensities are plotted on the same (vertical) scale to readily illustrate the relative yield of the two fractions (Fig. 7C–H). For example, proportionally more was produced at the lower temperature from OFMSW, while the opposite is true of the wood (Fig. 7C and D). This observation corroborates the TGA and Py-FID results which show greater OFMSW yields at lower temperature (Tables 1 and 2, Fig. 4).

For waste wood (with water), TD and pyrolysis traces (Fig. 7C) both reveal abundant lignin markers, with a proportionally higher content of longer-chain monomethoxyphenols (e.g., *trans*-isoeugenol), but also dimethoxyphenols (syringol and *trans*-syringylprop-2-ene) evident for the lower temperature run, the latter angiosperm-derived [59,61]. Lignin evidently begins to pyrolyze at the thermodesorption temperature (375 °C). Polysaccharides, on the other hand, appear to break down principally at higher temperatures, as their marker compounds are more abundant in the pyrolysis trace. The *n*-alkanes occur exclusively on the TD trace and likely arise from the finishing and/or binding waxes of the scrap wood (Sec. 2.1), although this was not separately investigated. Minor monoaromatic terpenoids and steroids appear on both chromatograms. Relatively more material is thermally desorbed from the waste wood hydrochar processed with whey, with notably more lignin markers, in particular vinylsyringol, *trans*-syringylprop-2-ene, and coniferyl alcohol (Fig. 7E). This observation is in concert with the shift of this sample's DTG maximum to a lower temperature (Sec. 3.2.1, Fig. 3B). Otherwise, the wood hydrochar pyrograms are fairly similar (Fig. 7C and E). Minor amounts of methyl- and dimethylurea were detected in both waste wood pyrolysis runs, likely from resin binders used in composite wood products. Organonitrogen compounds, in general, are very minor components in these thermodesorption and pyrolysis products, barely discernible at the scale employed in the total ion

Table 3
FTIR band assignments for Fig. 6, with their literature references.

cm^{-1}	Assignment	Comments	References
3350	O-H stretching	carboxylic acids, alcohols, phenols, water	[83–86]
3008	C-H stretching	alkene	[85–88]
2958	C-H asymmetric stretching of CH3	aliphatic stretching region	[85,87,88]
2924	C-H asymmetric stretching of CH2	aliphatic stretching region	[85,87,88]
2872	C-H symmetric stretching of CH3	aliphatic stretching region	[85,87,88]
2854	C-H symmetric stretching of CH2	aliphatic stretching region	[85,87,88]
2130	C=C=O? Inorganic?		[86]
2050	phenols? Inorganic?	weak.	[89]
1740	C=O stretching	ester carbonyl	[84–86]
1705	C=O stretching	carbonyl & carboxyl	[85,86]
1653	C=C stretching; Amide I	RHC=CHR & amide (protein) weak band	[85,86, 90–92]
1605	C=C ring stretching	aromatics	[83,86]
1541	Amide II	amide (protein) weak band	[90–92]
1515	C=C aromatic	aromatic	[83,89]
1464	C-H bending	alkane CH2 & CH3	[85,86,88]
1456	C-H bending	alkane CH2 & CH3	[83,85,86]
1430	CH2 & CH3 scissoring	lignins	[83]
1373	CH2 bending; CH scissoring		[83,88]
1335	CH2 out-of-plane; O-H scissoring	as with phenol	[83,89]
1319	CH2 scissoring; O-H scissoring		[83]
1280	C-O stretching	lignins & cellulose mannans	[83]
1232	C-O stretching	lignins, ester	[83,88]
1205	CH2 scissoring; O-H scissoring	as with phenol & eugenol	[83]
1163	C-O-C asymmetric stretching	C-O ester group	[83,85,88]
1116	C-O stretching; O-H stretching	C-O ester group, fatty acids	[83,85]
1072	C-O stretching		[83]
1041	C-O stretching; C-O-C symm. stretch.	polysaccharide C-O-C & C-OH	[83,84]
897	C-C stretching	polysaccharide (glucosidic rings)	[83]
870	C-C stretching	mannans	[83]
815	C-C stretching	mannans	[83]
668	aromatic?	toluene & phenol?	[89]

current chromatograms of Fig. 7. However, as a point of interest, *m/z* 70 mass chromatograms reveal that trace amounts of cyclic dipeptides are relatively more abundant in the wood + whey hydrochar thermodesorption products then they are in those of the wood + water sample (Supplemental Fig. S-1). These compounds are well-established markers for protein pyrolysis [62,63] and provide clues as to the influence of whey during HTC.

It was expected that the green waste from park maintenance, due to its abundance of woody material, would produce a hydrochar broadly similar to those of the waste wood. This is indeed the case, with a predominance of lignin and polysaccharide pyrolysis products (Fig. 7G). The TD trace reflects proportionally more angiosperm lignin-derived syringol derivatives and also relatively abundant sterols (notably, β-sitosterol) and triterpenes, while the pyrolyzate has a full series of minor *n*-alk-1-enes and alkanes.

As with the single-shot analysis of OFMSW, both double-shot chromatograms reveal a predominance of C_{16} and C_{18} fatty acids and esters, with relatively minor polysaccharide markers, steroids and normal hydrocarbons (Fig. 7B and D). Oleic acid (C18:1) predominates, as is characteristic of olive and sunflower oils [64,65]. Glyceryl monooleate was also detected by thermodesorption. The oils likely originate from the food scraps and residual cooking fats in the heterogenous organic waste. Grape pomace produced the other notably oleaginous hydrochar. Like the OFMSW, the pomace traces display abundant C_{16} and C_{18} fatty acids, but with relatively more ethyl esters and longer chain (even carbon number) acids and ethyl esters up to C_{32} (Fig. 7F). Unlike OFMSW, linoleic acid (C18:2) predominates, a marker for grapeseed oil [65]. Thermodesorption detected abundant β-sitosterol and an unidentified triterpene, while sequential pyrolysis shows a minor series of normal hydrocarbons. Both traces show very minor lignin and polysaccharide compounds. Winery pomace — the residue remaining after juice expression — includes grape skins, pulp, seeds, stems, and leaves, with the seeds likely responsible for most of the oil.

The oak wood biochar, a biomass torrefaction product presented here for comparison with the hydrochars, produced little except minor terpenoids during thermodesorption (Fig. 7H). Upon pyrolysis, it yields mostly phenol and mono-, di-, and triaromatic hydrocarbons, notably benzene, toluene, 1,7-dimethylphenanthrene, and retene, the latter being characteristic of wood smoke [66] and by extension, charred wood. Its TD- and Py-GC-MS fingerprints bear no resemblance to those of the hydrochars, corroborating the dissimilarity already noted (Sections 3.1.1, 3.2.1., Figs. 2 and 3).

4. Discussion

4.1. General chemical characteristics of waste-based hydrochars

The multi-pronged approach to the characterization of the five waste-based hydrochars presented a consistent picture indicating two general types — “oily” and “woody".

The two “oily” hydrochars (OFMSW and pomace) and their raw feedstocks were shown to be lipid-rich and contrast with the other “woody” hydrochars as follows:

- Higher molar H/C ratios (Table 1, Fig. 2, Sec. 3.1.1)
- Greater yield at lower TGA pyrolysis temperature (Table 1, Figs. 3 and 4, Sec. 3.2)
- Via Py-FID/TCD, more S1 and proportionally more CO_2 than CO (Table 2, Figs. 4 and 5, Sec. 3.3)
- More prominent aliphatic FTIR bands (Fig. 6, Sec. 3.4)
- Strong predominance of fatty acids and their derivatives in the TE-Py-GC-MS results (Fig. 7B–D, F, Sec. 3.5).

Among the “woody” lignocellulosic group (groundskeeping waste and scrap wood hydrochars), details notable on the TE-Py-GC-MS traces are significant. Levoglucosan is consistently the predominant polysaccharide marker compound for these samples, recognized as a characteristic pyrolysis product of cellulose and starch – e.g., Refs. [67–69]. Furfural is considered a pyrolysis marker compound for pentosan polysaccharides, particularly angiosperm hemicellulose [70–72]. However, by TE-Py-GC-MS it appears as only a minor component of the woody hydrochars (Fig. 7). One explanation is that the more labile hemicellulose had already been depolymerized in the HTC process (Sec. 3.2.2, Fig. 4A and B). It could also be that hardwoods comprise a only a minor fraction of the waste wood, as suggested by the low abundance of syringols in the analytical pyrolysis results. A botanical classification of the woods in the raw feedstock was beyond the scope of the project, but in future work, plans should be made to also analyze the feedstock by TE-Py-GC-MS.

A notable feature of the Py-IRD data is the difference in the proportions of CO_2 and CO evolved during pyrolysis as well as combustion (Table 2, Fig. 5C and D). The preference for CO_2 in OFMSW hydrochar correlates with its abundance of carbonyl compounds (fatty acids and esters), whereas there was relatively more CO produced from the wood hydrochar, notable for ether linkages and hydroxyl functions in lignocellulose (Fig. 6C and 7A – D).

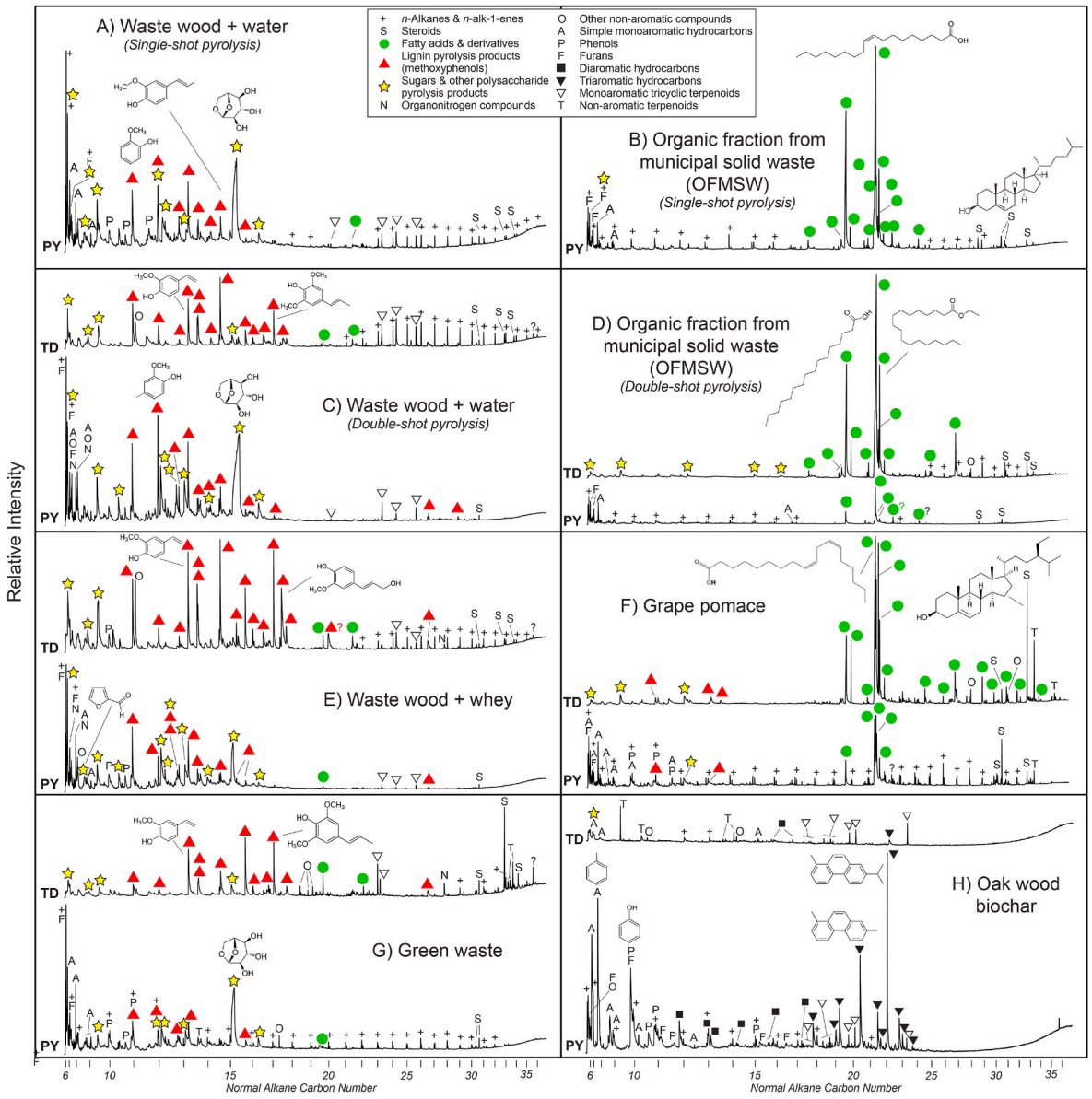

Fig. 7. Thermodesorption- and pyrolysis-GC-MS total ion chromatograms for the five hydrochars and biochar. A and B) "Single-shot" pyrograms acquired at the 610 °C pyrolysis temperature. C–H) "Double-shot" chromatograms acquired by thermodesorption at 350 °C (upper traces) and by subsequent pyrolysis of the thermodesorption residue at 610 °C (lower traces). For each pair of TD and Py traces, the intensities are plotted on the same (vertical) scale, graphically illustrating the relative yields of the two runs.

4.2. Hydrochar vs. biochar

By all analytical methods employed herein, the oak wood biochar (torrefied dry at high temperature) contrasts strongly with the hydrochars (products of comparatively mild hydrothermal carbonization), including those prepared from wood. This is evident beginning with the biochar's low volatile matter and high fixed carbon percentages, low H/C and O/C ratios, and modest mass loss during TGA (Table 1, Figs. 2 and 3A). The FTIR spectrum of this biochar displays mostly aromatic C=C bands [31]. Upon thermodesorption the biochar yielded little beyond minor terpenoids, while mono- and triaromatic compounds dominate its pyrolyzate (Fig. 7H–Sec. 3.5.2). It shows none of the lignocellulosic marker compounds characteristic of the woody hydrochars, nor the lipids abundant in the oily samples (Fig. 7).

Hydrochar and torrefied biochar represent two important methods for valorizing organic wastes, producing very distinctive products, each with its own special applications and potential for creative usage. In Section 4.3, we evaluate potential uses for hydrochars produced from a variety of biomass feedstocks.

4.3. Biofuel and other possible applications of hydrochar

The extraordinarily high HAWK Production and Oil Saturation Indices of the OFMSW hydrochar draw attention to its potential oil-producing capabilities, confirmed by the abundance of lipids seen on its TD-Py-GC-MS traces (Table 2, Fig. 7B–D). The pomace hydrochar is similarly rich in fatty acids, although with a distinctive distribution (Fig. 7F). While labile pseudo-components (305 °C, Fig. 4A and B) were reduced by the HTC process, the resulting hydrochars remain lipid-rich. Both the OFMSW and pomace hydrochars have a preponderance of lipids in the C_{16}–C_{18} range, appropriate for biodiesel source material.

The evidence suggests a potential to produce liquid biofuels as petroleum product replacement, but the optimum upgrading method remains to be determined. The thermal desorption results show that the

lipids are already partially esterified (Sec. 3.5.2), a step closer to being useful as biodiesel. For a more complete conversion, a more complete esterification would be needed, or alternatively processes including decarboxylation, solvent extraction, catalysis, and/or distillation could be employed. One possible way forward would be to use higher temperatures and pressures for hydrothermal liquefaction, rather than the mild hydrothermal carbonization process employed [73–75]. This should be the subject of future research, which could also include quantitative TD- and Py-GC-MS with the objective of developing predictive capabilities for the product yields of the various types of waste.

The compositions of the woody hydrochars suggest potential application as feedstock for obtaining valuable bio-refinery platform chemicals, including methoxyphenols and anhydrosugars (Fig. 7A–C, E, G) as substitutes for primary petrochemicals. Among methoxyphenols, guaiacol is of particular interest as chemical precursor, for example, in the production of vanillin [76]. Vanillin itself was not detected in the hydrochars, likely because it is thermally labile [77] and may have been lost during HTC. Petrovič et al. [15,16] recognized the catalytic role of acidic cheese whey in the hydrothermal carbonization process. It dramatically increased the yield of longer-chain methoxyphenols from the waste wood (Fig. 7C–E), of potential benefit in the production of platform chemicals, as well as avoiding the environmentally problematic disposal of whey. Again, while we note the desirability of a more quantitative, predictive approach in order to fully implement the potential of this method, the basic insights presented herein are compelling nonetheless.

The anhydrosugar levoglucosan is the most abundant polysaccharide pyrolysis product of the woody hydrochars. It is of increasing interest as a platform compound for the synthesis of polymers and sorbitol substitute, for example [78–80]. Furfural is another biomass-derived compound of industrial interest [71,76,81], but was only a minor compound in the hydrochars, likely being too labile and lost during HTC (Sec. 4.1).

In creating biomass-based petroleum product substitutes, it is important not to generate new hazardous materials. Fortunately, polycyclic aromatic hydrocarbons were not detected in the hydrochars (Fig. 7), but the scrap wood does contain significant amounts of lead, likely from paint, while the grape pomace has elevated copper concentrations [31].

5. Conclusions

Hydrothermal carbonization, a “mild” hydrous pyrolysis process, demonstrates its promise as a means to valorize solid organic wastes and thereby reduce the need for landfills and provide substitutes for petroleum derivatives. Five hydrochars were prepared from “real world” heterogenous waste materials at pilot plant scale, including scrap wood (processed separately with tap water and caseiculture whey), winery pomace, groundskeeping trimmings, and the organic fraction (largely food scraps) of municipal wastes. These were compared with a commercial torrefied wood biochar.

Organic geochemical techniques traditionally applied in advanced characterization of fossil fuels, including proximate & ultimate analyses, TGA, FTIR, quantitative Py-FID/IRD, and TE-Py-GC-MS, were shown to be effective for elucidating hydrochar and biochar composition. This opened new possibilities for the study of these products in detail, including diverse applications such as tracking the evolution of different feedstock materials after carbonization, the possible uses as biofuels and alternative chemical feedstocks, and the identification of potential pollutants.

The molecular composition of hydrochar was strongly influenced by feedstock type. Of the five hydrochars, two (OFMSW and pomace) are lipid-rich and classified as “oily”, suggesting potential as biodiesel precursors. The other three, herein termed “woody”, are possible lignocellulosic sources for valuable platform chemicals for the expanding biorefinery industry. These hydrochars have little in common chemically with the torrefied biochar, which is highly carbonized and refractory. Hydrochars also perform well as soil amendments in support of bioremediation of contaminants, an aspect previously presented in detail [31].

For future work, we recommend characterization by Py-FID/IRD (as with HAWK® or Rock-Eval® instruments) using a constant rate of increase across the full pyrolysis temperature range, along with “double-shot” TD-Py-GC-MS for thorough organic molecular fingerprinting. This should be done on both the raw feedstock and the hydrochars, the latter from experiments done under various temperature and pressure conditions. Furthermore, the TD- and Py-GC-MS analyses should be performed with internal standards to develop a more rigorously quantitative approach with predictive capabilities.

CRediT authorship contribution statement

Michael A. Kruge: Writing – original draft, Visualization, Methodology, Investigation, Formal analysis, Data curation, Conceptualization. **Teresa A. Centeno:** Writing – review & editing, Supervision, Resources, Funding acquisition, Conceptualization. **Álvaro Amado-Fierro:** Writing – review & editing, Visualization, Investigation, Data curation. **José Manuel González-LaFuente:** Writing – review & editing, Resources, Funding acquisition. **Rubén Forján:** Writing – review & editing, Investigation. **José Luis R. Gallego:** Writing – original draft, Supervision, Funding acquisition, Formal analysis, Conceptualization.

Declaration of competing interest

The authors declare that they have no known competing financial interests or personal relationships that could have appeared to influence the work reported in this paper.

Acknowledgements

This study was carried out with the support of COGERSA, which supplied the waste materials (together with Bodegas Monasterio de Corias and Quesería La Borbolla), as well as steam, electricity and water for the operation of the HTC pilot reactor. We are grateful to Julie Jones, Albert Maende, and Dan Jarvie of Wildcat Technologies, LLC for kindly analyzing our samples on the HAWK pyrolysis instrument.

The authors would like also to thank Dr. María Antonia Díez Díaz-Estébanez for lending her thermogravimetric analyzer for the determination of pyrolysis thermograms.

This research was partially supported by the European Union’s Horizon 2020 research and innovation program, under grant agreement No. 101006656 (GICO Project), the Plan de Ciencia, Tecnología e Innovación (PCTI) 2018–2022 del Principado de Asturias, the ERDF (project IDI/2021/000037), and the NANOCAREM and INTERSOIL projects (PID2019-106939 GB-I00 and PID2023-147718NB-I00, AEI/Spain, FEDER/EU).

Appendix A. Supplementary data

Supplementary data to this article can be found online at https://doi.org/10.1016/j.biombioe.2025.108706.

Data availability

Data will be made available on request.

References

[1] S. Kaza, L.C. Yao, P. Bhada-Tata, F. Van Woerden, What a Waste 2.0: a Global Snapshot of Solid Waste Management to 2050, World Bank, Washington, DC, 2018, p. 38.

[2] J. Quereda Sabater, «¿Dónde va qué?». Los problemas de la regulación jurídica de la obligación de entrega separada de residuos domésticos: Certezas, dudas e

insuficiencias, Cuadernos Derecho Local 65 (2024) 238, https://doi.org/10.61521/cuadernosderecholocal.65.975.
[3] WHO, Solid waste, in: Compendium of WHO and Other UN Guidance in Health and Environment, 2024 Update, World Health Organization, Geneva, 2024, p. 12. https://iris.who.int/handle/10665/378095.
[4] E. Lizundia, F. Luzi, D. Puglia, Organic waste valorisation towards circular and sustainable biocomposites, Green Chem. 24 (2022) 5429, https://doi.org/10.1039/d2gc01668k.
[5] L. Campion, M. Bekchanova, R. Malina, T. Kuppens, The costs and benefits of biochar production and use: a systematic review, J. Clean. Prod. 408 (2023) 137138, https://doi.org/10.1016/j.jclepro.2023.137138.
[6] R.T. Koide, B.T. Nguyen, R.H. Skinner, C.J. Dell, M.S. Peoples, P.R. Adler, P. J. Drohan, Biochar amendment of soil improves resilience to climate change, GCB Bioenergy 7 (2015) 1084, https://doi.org/10.1111/gcbb.12191.
[7] M. Lebrun, R. Nandillon, F. Miard, S. Bourgerie, D. Morabito, Biochar assisted phytoremediation for metal(loid) contaminated soils, in: V. Pandey (Ed.), Assisted Phytoremediation, Elsevier, Amsterdam, 2022, p. 101, https://doi.org/10.1016/B978-0-12-822893-7.00010-0.
[8] S. Haghighi Mood, M.R. Pelaez-Samaniego, M. Garcia-Perez, Perspectives of engineered biochar for environmental applications: a review, Energy Fuels 36 (2022) 7940, https://doi.org/10.1021/acs.energyfuels.2c01201.
[9] S. Sachdeva, R. Kumar, P.K. Sahoo, A.K. Nadda, Recent advances in biochar amendments for immobilization of heavy metals in an agricultural ecosystem: a systematic review, Environ. Pollut. 319 (2023) 120937, https://doi.org/10.1016/j.envpol.2022.120937.
[10] S.P. Singh Yadav, S. Bhandari, D. Bhatta, A. Poudel, S. Bhattarai, P. Yadav, N. Ghimire, P. Paudel, P. Paudel, J. Shrestha, B. Oli, Biochar application: a sustainable approach to improve soil health, J. Agric. Food Res. 11 (2023) 100498, https://doi.org/10.1016/j.jafr.2023.100498.
[11] M. Cavali, N. Libardi Junior, J.D. de Sena, A.L. Woiciechowski, C.R. Soccol, P. Belli Filho, R. Bayard, H. Benbelkacem, A.B. de Castilhos Junior, A review on hydrothermal carbonization of potential biomass wastes, characterization and environmental applications of hydrochar, and biorefinery perspectives of the process, Sci. Total Environ. 857 (2023) 159627, https://doi.org/10.1016/j.scitotenv.2022.159627.
[12] J.O. Ighalo, S. Rangabhashiyam, K. Dulta, C.T. Umeh, K.O. Iwuozor, C.O. Aniagor, S.O. Eshiemogie, F.U. Iwuchukwu, C.A. Igwegbe, Recent advances in hydrochar application for the adsorptive removal of wastewater pollutants, Chem. Eng. Res. Des. 184 (2022) 419, https://doi.org/10.1016/j.cherd.2022.06.028.
[13] M. Liu, G.A.G. Kavindi, Z. Lei, Environmental sustainability-based comparison for production, properties, and applications of biochar and hydrochar, in: H.H. Ngo, W. Guo, A. Pandey, S. Varjani, D.C.W. Tsang (Eds.), Current Developments in Biotechnology and Bioengineering, Elsevier, Amsterdam, 2023, p. 387, https://doi.org/10.1016/B978-0-323-91873-2.00012-1.
[14] R.B. Madsen, M.M. Jensen, M. Glasius, Qualitative characterization of solid residue from hydrothermal liquefaction of biomass using thermochemolysis and stepwise pyrolysis-gas chromatography-mass spectrometry, Sustain. Energy Fuels 1 (2017) 2110, https://doi.org/10.1039/C7SE00357A.
[15] A. Petrovič, T. Cenčič Predikaka, S. Vohl, G. Hostnik, M. Finšgar, L. Čuček, Hydrothermal conversion of oilseed cakes into valuable products: influence of operating conditions and whey as an alternative process liquid on product properties and their utilization, Energy Convers. Manag. 313 (2024) 118640, https://doi.org/10.1016/j.enconman.2024.118640.
[16] A. Petrovič, S. Vohl, S. Gruber, K. Rola, T.C. Predikaka, L. Čuček, D. Urbancl, Thermogravimetric, kinetic and thermodynamic behaviour of raw and hydrothermally pretreated oil cakes during pyrolysis and TG-FTIR analysis of the gaseous products, Renew. Energy (2025) 123041, https://doi.org/10.1016/j.renene.2025.123041.
[17] B. Seshadri, N.S. Bolan, R. Thangarajan, U. Jena, K.C. Das, H. Wang, R. Naidu, Biomass energy from revegetation of landfill sites, in: M.N.V. Prasad (Ed.), Bioremediation and Bioeconomy, Elsevier, Amsterdam, 2016, p. 99, https://doi.org/10.1016/B978-0-12-802830-8.00005-8.
[18] M. Aliyu, B.R. Moser, F.A. Alharthi, U. Rashid, Efficient production of biodiesel from palm fatty acid distillate using a novel hydrochar-based solid acid catalyst derived from palm leaf waste, Process Saf. Environ. Prot. 187 (2024) 1126, https://doi.org/10.1016/j.psep.2024.05.040.
[19] M.M. Santos, A.L. Marques Sierra, Á. Amado-Fierro, M. Suárez, F. Blanco, J.M.G. La Fuente, M.A. Diez, T.A. Centeno, Reducing cement consumption in mortars by waste-derived hydrochars, J. Build. Eng. 75 (2023) 106987, https://doi.org/10.1016/j.jobe.2023.106987.
[20] A. Dieguez-Alonso, A. Funke, A. Anca-Couce, A.G. Rombolà, G. Ojeda, J. Bachmann, F. Behrendt, Towards biochar and hydrochar engineering—Influence of process conditions on surface physical and chemical properties, thermal stability, nutrient availability, toxicity and wettability, Energies 11 (2018) 496, https://doi.org/10.3390/en11030496.
[21] H.S. Kambo, A. Dutta, A comparative review of biochar and hydrochar in terms of production, physico-chemical properties and applications, Renew. Sustain. Energy Rev. 45 (2015) 359, https://doi.org/10.1016/j.rser.2015.01.050.
[22] S. Kang, X. Li, J. Fan, J. Chang, Characterization of hydrochars produced by hydrothermal carbonization of lignin, cellulose, d-xylose, and wood meal, Ind. Eng. Chem. Res. 51 (2012) 9023, https://doi.org/10.1021/ie300565d.
[23] M.F. Aller, Biochar properties: transport, fate, and impact, Crit. Rev. Environ. Sci. Technol. 46 (2016) 1183, https://doi.org/10.1080/10643389.2016.1212368.
[24] A. Kumar, K. Saini, T. Bhaskar, Hydrochar and biochar: production, physicochemical properties and techno-economic analysis, Bioresour. Technol. 310 (2020) 123442, https://doi.org/10.1016/j.biortech.2020.123442.
[25] B. Zhang, B.K. Biswal, J. Zhang, R. Balasubramanian, Hydrothermal treatment of biomass feedstocks for sustainable production of chemicals, fuels, and materials: progress and perspectives, Chem. Rev. 123 (2023) 7193, https://doi.org/10.1021/acs.chemrev.2c00673.
[26] Z. Zhang, Z. Zhu, B. Shen, L. Liu, Insights into biochar and hydrochar production and applications: a review, Energy 171 (2019) 581, https://doi.org/10.1016/j.energy.2019.01.035.
[27] F. Behar, V. Beaumont, H.L. De B. Penteado, Rock-eval 6 technology: performances and developments, Oil Gas Sci. Technol. Rev. IFP 56 (2001) 111, https://doi.org/10.2516/ogst:2001013.
[28] K.E. Peters, Guidelines for evaluating petroleum source rock using programmed pyrolysis, AAPG Bull. 70 (1986) 318, https://doi.org/10.1306/94885688-1704-11D7-8645000102C1865D.
[29] M.A. Kruge, J.L.R. Gallego, A. Lara-Gonzalo, N. Esquinas, Environmental forensics study of crude oil and petroleum product spills in coastal and oilfield settings: combined insights from conventional GC–MS, thermodesorption–GC–MS, and pyrolysis–GC–MS, in: S.A. Stout, Z. Wang (Eds.), Oil Spill Environmental Forensics Case Studies, Butterworth-Heinemann, Oxford, 2018, p. 131, https://doi.org/10.1016/B978-0-12-804434-6.00007-0.
[30] M.A. Kruge, A. Lara-Gonzalo, J.L.R. Gallego, Environmental forensics of complexly contaminated sites: a complimentary fingerprinting approach, Environ. Pollut. 263 (2020) 114645, https://doi.org/10.1016/j.envpol.2020.114645.
[31] Á. Amado-Fierro, T.A. Centeno, J.L.R. Gallego, R. Forján, Critical assessment of biowaste-derived hydrochars for remediating contaminated soils, Environ. Technol. Innov. 38 (2025) 104183, https://doi.org/10.1016/j.eti.2025.104183.
[32] M. Kruge, T.A. Centeno, Á. Amado-Fierro, J.M. González-LaFuente, R. Forján, J. R. Gallego, in: Hydrothermal Carbonization of Biomass Wastes: Sustainability and Geochemistry, at 31st International Meeting on Organic Geochemistry (IMOG 2023), 2023, https://doi.org/10.3997/2214-4609.202333058. Montpellier, France.
[33] A. Maende, A. Pepper, D.M. Jarvie, W.D. Weldon, Advanced pyrolysis data and interpretation methods to identify unconventional reservoir sweet spots in fluid phase saturation and fluid properties (API gravity) from drill cuttings and cores. Search and discovery article #80596. At AAPG 2017 Annual Convention, 2017. Houston (TX), http://www.searchanddiscovery.com/pdfz/documents/2017/80596maende/ndx_maende.pdf.html.
[34] J. Espitalié, G. Deroo, F. Marquis, La pyrolyse Rock-Eval et ses applications. Première partie, Rev. Inst. Fr. Pét. 40 (1985) 563, https://doi.org/10.2516/ogst:1985035.
[35] E. Lafargue, F. Marquis, D. Pillot, Rock-eval 6 applications in hydrocarbon exploration, production and in soil contamination studies, Rev. Inst. Fr. Pét. 53 (1998) 421, https://doi.org/10.2516/ogst:1998036.
[36] J. Parikh, S.A. Channiwala, G.K. Ghosal, A correlation for calculating HHV from proximate analysis of solid fuels, Fuel 84 (2005) 487, https://doi.org/10.1016/j.fuel.2004.10.010.
[37] Z. Chen, M. Hu, X. Zhu, D. Guo, S. Liu, Z. Hu, B. Xiao, J. Wang, M. Laghari, Characteristics and kinetic study on pyrolysis of five lignocellulosic biomass via thermogravimetric analysis, Bioresour. Technol. 192 (2015) 441, https://doi.org/10.1016/j.biortech.2015.05.062.
[38] F. de Campos Vitorino, M. Nazarkovsky, A. Azadeh, C. Martins, B.M. da Cunha Gomes, J. Dweck, R.D.T. Filho, H. Savastano, Bamboo phase quantification using thermogravimetric analysis: deconvolution and machine learning, Cellulose 30 (2023) 1873, https://doi.org/10.1007/s10570-022-04921-y.
[39] M. Hu, Z. Chen, S. Wang, D. Guo, C. Ma, Y. Zhou, J. Chen, M. Laghari, S. Fazal, B. Xiao, B. Zhang, S. Ma, Thermogravimetric kinetics of lignocellulosic biomass slow pyrolysis using distributed activation energy model, Fraser–Suzuki deconvolution, and iso-conversional method, Energy Convers. Manag. 118 (2016) 1, https://doi.org/10.1016/j.enconman.2016.03.058.
[40] C. Ma, Y. Yu, C. Tan, J. Hu, H. Wang, Kinetics, reaction mechanism and product distribution of lignocellulosic biomass pyrolysis using triple-parallel reaction model, combined kinetics, Py-GC/MS, and artificial neural networks, Ind. Crops Prod. 224 (2025) 120308, https://doi.org/10.1016/j.indcrop.2024.120308.
[41] A.K. Burnham, B.J. Schmidt, R.L. Braun, A test of the parallel reaction model using kinetic measurements on hydrous pyrolysis residues, Org. Geochem. 23 (1995) 931, https://doi.org/10.1016/0146-6380(95)00069-0.
[42] B.P. Tissot, R. Pelet, P.H. Ungerer, Thermal history of sedimentary basins, maturation indices, and kinetics of oil and gas generation, AAPG Bull. 71 (1987) 1445, https://doi.org/10.1306/703C80E7-1707-11D7-8645000102C1865D.
[43] D. Sebag, E.P. Verrecchia, L. Cécillon, T. Adatte, R. Albrecht, M. Aubert, F. Bureau, G. Cailleau, Y. Copard, T. Decaens, J.R. Disnar, M. Hetényi, T. Nyilas, L. Trombino, Dynamics of soil organic matter based on new Rock-Eval indices, Geoderma 284 (2016) 185, https://doi.org/10.1016/j.geoderma.2016.08.025.
[44] F. Baudin, J.-R. Disnar, A. Aboussou, F. Savignac, Guidelines for Rock–Eval analysis of recent marine sediments, Org. Geochem. 86 (2015) 71, https://doi.org/10.1016/j.orggeochem.2015.06.009.
[45] J. Carrie, H. Sanei, G. Stern, Standardisation of Rock–Eval pyrolysis for the analysis of recent sediments and soils, Org. Geochem. 46 (2012) 38, https://doi.org/10.1016/j.orggeochem.2012.01.011.
[46] L. Cécillon, F. Baudin, C. Chenu, S. Houot, R. Jolivet, T. Kätterer, S. Lutfalla, A. Macdonald, F. van Oort, A.F. Plante, F. Savignac, L.N. Soucémarianadin, P. Barré, A model based on Rock-Eval thermal analysis to quantify the size of the centennially persistent organic carbon pool in temperate soils, Biogeosciences 15 (2018) 2835, https://doi.org/10.5194/bg-15-2835-2018.
[47] J.R. Disnar, B. Guillet, D. Keravis, C. Di-Giovanni, D. Sebag, Soil organic matter (SOM) characterization by Rock-Eval pyrolysis: scope and limitations, Org. Geochem. 34 (2003) 327, https://doi.org/10.1016/S0146-6380(02)00239-5.

[48] V. Ducasse, F. Watteau, I. Kowalewski, H. Ravelojaona, Y. Capowiez, J. Peigné, The amending potential of vermicompost, compost and digestate from urban biowaste: evaluation using biochemical, Rock-Eval® thermal analyses and transmission electronic microscopy, Bioresour. Technol. Rep. 22 (2023) 101405, https://doi.org/10.1016/j.biteb.2023.101405.
[49] J. Jacob, F. Delarue, Y. Copard, C. Le Milbeau, L. Grasset, P. Brockmann, Comparison between Rock-Eval® and temperature-programmed pyrolysis/mass spectrometry for the analysis of environmental and geological samples, J. Anal. Appl. Pyrolysis 173 (2023) 106078, https://doi.org/10.1016/j.jaap.2023.106078.
[50] I. Kowalewski, Rock-Eval®: supporting soil research for the climate challenge. https://www.ifpenergiesnouvelles.com/brief/rock-evalr-supporting-soil-research-climate-challenge, 2021. (Accessed 27 February 2024).
[51] L. Pacini, T. Adatte, P. Barré, M. Boussafir, N. Bouton, L. Cécillon, V. Lamoureux-Var, D. Sebag, E. Verrecchia, A. Wattripont, F. Baudin, Reproducibility of Rock-Eval® thermal analysis for soil organic matter characterization, Org. Geochem. 186 (2023) 104687, https://doi.org/10.1016/j.orggeochem.2023.104687.
[52] D. Sebag, M. Debret, M. M'voubou, R.M. Obame, A. Ngomanda, R. Oslisly, I. Bentaleb, J.-R. Disnar, P. Giresse, Coupled Rock-Eval pyrolysis and spectrophotometry for lacustrine sedimentary dynamics: application for West Central African rainforests (Kamalété and Nguène lakes, Gabon), Holocene 23 (2013) 1173, https://doi.org/10.1177/0959683613483622.
[53] D. Sebag, J.R. Disnar, B. Guillet, C. Di Giovanni, E.P. Verrecchia, A. Durand, Monitoring organic matter dynamics in soil profiles by 'Rock-Eval pyrolysis': bulk characterization and quantification of degradation, Eur. J. Soil Sci. 57 (2006) 344, https://doi.org/10.1111/j.1365-2389.2005.00745.x.
[54] S. Killops, V. Killops, Introduction to Organic Geochemistry, second ed., Blackwell, Oxford, 2005, p. 393.
[55] B.P. Tissot, D.H. Welte, Petroleum Formation and Occurrence, Springer, Berlin, 1984, p. 702.
[56] A.W. Gillespie, H. Sanei, A. Diochon, B.H. Ellert, T.Z. Regier, D. Chevrier, J. J. Dynes, C. Tarnocai, E.G. Gregorich, Perennially and annually frozen soil carbon differ in their susceptibility to decomposition: analysis of Subarctic earth hummocks by bioassay, XANES and pyrolysis, Soil Biol. Biochem. 68 (2014) 106, https://doi.org/10.1016/j.soilbio.2013.09.021.
[57] Á. Amado-Fierro, T. Offermans, J. Jansen, T.A. Centeno, M.A. Díez, Chemometrics to connect feedstock quality, process settings and calorific value of hydrochar through infrared spectra, Fuel Process. Technol. 271 (2025) 108201, https://doi.org/10.1016/j.fuproc.2025.108201.
[58] M.A. Kruge, Analytical pyrolysis principles and applications to environmental science, in: M. Barbooti (Ed.), Environmental Applications of Instrumental Chemical Analysis, CRC Press, Boca Raton (FL), 2015, p. 533. https://digitalcommons.montclair.edu/earth-environ-studies-facpubs/66/.
[59] A.D. Pouwels, A. Tom, G.B. Eijkel, J.J. Boon, Characterisation of beech wood and its holocellulose and xylan fractions by pyrolysis-gas chromatography-mass spectrometry, J. Anal. Appl. Pyrolysis 11 (1987) 417, https://doi.org/10.1016/0165-2370(87)85045-3.
[60] C. Saiz-Jimenez, J.W. De Leeuw, Lignin pyrolysis products: their structures and their significance as biomarkers, Org. Geochem. 10 (1986) 869, https://doi.org/10.1016/S0146-6380(86)80024-9.
[61] O. Faix, D. Meier, I. Grobe, Studies on isolated lignins and lignins in woody materials by pyrolysis-gas chromatography-mass spectrometry and off-line pyrolysis-gas chromatography with flame ionization detection, J. Anal. Appl. Pyrolysis 11 (1987) 403, https://doi.org/10.1016/0165-2370(87)85044-1.
[62] B.A. Stankiewicz, P.F. van Bergen, I.J. Duncan, J.F. Carter, D.E.G. Briggs, R. P. Evershed, Recognition of chitin and proteins in invertebrate cuticles using analytical pyrolysis/gas chromatography and pyrolysis/gas chromatography/mass spectrometry, Rapid Comm. Mass Spectrom. 10 (1996) 1747, https://doi.org/10.1002/(SICI)1097-0231(199611)10:14<1747::AID-RCM713>3.0.CO;2-H.
[63] X. Zang, J.D.H. van Heemst, K.J. Dria, P.G. Hatcher, Encapsulation of protein in humic acid from a histosol as an explanation for the occurrence of organic nitrogen in soil and sediment, Org. Geochem. 31 (2000) 679, https://doi.org/10.1016/S0146-6380(00)00040-1.
[64] G. Beltrán, C. del Rio, S. Sánchez, L. Martínez, Influence of harvest date and crop yield on the fatty acid composition of virgin olive oils from Cv. Picual, J. Agric. Food Chem. 52 (2004) 3434, https://doi.org/10.1021/jf049894n.
[65] USDA, FoodData central. https://fdc.nal.usda.gov, 2019. (Accessed 7 April 2025).
[66] B.R.T. Simoneit, W.F. Rogge, M.A. Mazurek, L.J. Standley, L.M. Hildemann, G. R. Cass, Lignin pyrolysis products, lignans, and resin acids as specific tracers of plant classes in emissions from biomass combustion, Environ. Sci. Technol. 27 (1993) 2533, https://doi.org/10.1021/es00048a034.
[67] W.-H. Chen, C.-W. Wang, H.C. Ong, P.L. Show, T.-H. Hsieh, Torrefaction, pyrolysis and two-stage thermodegradation of hemicellulose, cellulose and lignin, Fuel 258 (2019) 116168, https://doi.org/10.1016/j.fuel.2019.116168.
[68] C.M. Lakshmanan, H.E. Hoelscher, Production of Levoglucosan by Pyrolysis of Carbohydrates Pyrolysis in Hot Inert Gas Stream, 22, 1970, p. 261, https://doi.org/10.1002/star.19700220804.
[69] S. Maduskar, V. Maliekkal, M. Neurock, P.J. Dauenhauer, On the yield of levoglucosan from cellulose pyrolysis, ACS Sustainable Chem. Eng. 6 (2018) 7017, https://doi.org/10.1021/acssuschemeng.8b00853.
[70] J. Berglund, D. Mikkelsen, B.M. Flanagan, S. Dhital, S. Gaunitz, G. Henriksson, M. E. Lindström, G.E. Yakubov, M.J. Gidley, F. Vilaplana, Wood hemicelluloses exert distinct biomechanical contributions to cellulose fibrillar networks, Nat. Commun. 11 (2020) 4692, https://doi.org/10.1038/s41467-020-18390-z.
[71] C.M. Cai, T. Zhang, R. Kumar, C.E. Wyman, Integrated furfural production as a renewable fuel and chemical platform from lignocellulosic biomass, J. Chem. Technol. Biotechnol. 89 (2014) 2, https://doi.org/10.1002/jctb.4168.
[72] F.-X. Collard, J. Blin, A review on pyrolysis of biomass constituents: mechanisms and composition of the products obtained from the conversion of cellulose, hemicelluloses and lignin, Renew. Sustain. Energy Rev. 38 (2014) 594, https://doi.org/10.1016/j.rser.2014.06.013.
[73] J. Akhtar, N.A.S. Amin, A Review on Process Conditions for Optimum bio-oil Yield in Hydrothermal Liquefaction of Biomass, 15, 2011, p. 1615, https://doi.org/10.1016/j.rser.2010.11.054.
[74] M. Déniel, G. Haarlemmer, A. Roubaud, E. Weiss-Hortala, J. Fages, Energy valorisation of food processing residues and model compounds by hydrothermal liquefaction, Renew. Sustain. Energy Rev. 54 (2016) 1632, https://doi.org/10.1016/j.rser.2015.10.017.
[75] J.A. Ramirez, R.J. Brown, T.J. Rainey, A review of hydrothermal liquefaction bio-crude properties and prospects for upgrading to transportation fuels, Energies 8 (2015) 6765, https://doi.org/10.3390/en8076765.
[76] S.H. Shinde, A. Hengne, C.V. Rode, Lignocellulose-derived platform molecules: an introduction, in: S. Saravanamurugan, A. Pandey, H. Li, A. Riisager (Eds.), Biomass, Biofuels, Biochemicals, Elsevier, Amsterdam, 2020, p. 1, https://doi.org/10.1016/B978-0-444-64307-0.00001-9.
[77] J. Hao, F. Xu, D. Yang, B. Wang, Y. Qiao, Y. Tian, Analytical pyrolysis of biomass using pyrolysis-gas chromatography/mass spectrometry, Renew. Sustain. Energy Rev. 208 (2025) 115090, https://doi.org/10.1016/j.rser.2024.115090.
[78] A. Hamid, A. Alam, L. Ali, T. Shittu, F.G.T. Labata, M. Altarawneh, Improving the yield of levoglucosan platform chemical from the pyrolysis of date pits waste biomass through pre-treatments, Sustain. Chem. Pharm. 42 (2024) 101758, https://doi.org/10.1016/j.scp.2024.101758.
[79] I. Itabaiana Junior, M. Avelar do Nascimento, R.O.M.A. de Souza, A. Dufour, R. Wojcieszak, Levoglucosan: a promising platform molecule? Green Chem. 22 (2020) 5859, https://doi.org/10.1039/D0GC01490G.
[80] E.G. Silveira Junior, T.d.C. Silveira, V.H. Perez, O.R. Justo, G.F. David, S. A. Fernandes, Fast pyrolysis of elephant grass: intensification of levoglucosan yield and other value-added pyrolytic by-products, J. Energy Inst. 101 (2022) 254, https://doi.org/10.1016/j.joei.2022.02.003.
[81] N. Wu, A.E. Leon, S. Ghysels, J. Pieters, F. Ronsse, High furfural and levoglucosan selectivity from stepwise torrefaction and fast pyrolysis of sugarcane trash washed with citric acid, Energy Convers. Manag. 301 (2024) 118065, https://doi.org/10.1016/j.enconman.2024.118065.
[82] J. Koppejan, S. van Loo, The Handbook of Biomass Combustion and Co-firing, Routledge, London, 2007, p. 464.
[83] O. Dirckx, M.C. Triboulot-Trouy, A. Merlin, X. Deglise, Modifications de la couleur du bois d'Abies grandis exposé à la lumière solaire, Ann. For. Sci. 49 (1992) 425, https://doi.org/10.1051/forest:19920501.
[84] E.R. Durango Padilla, F.A.S. Hansted, C.M.R. Luna, C.I. de Campos, F.M. Yamaji, Biochar derived from agricultural waste and its application as energy source in blast furnace, Renew. Energy 220 (2024) 119688, https://doi.org/10.1016/j.renene.2023.119688.
[85] M.-A. Poiana, E. Alexa, M.-F. Munteanu, R. Gligor, D. Moigradean, C. Mateescu, Use of ATR-FTIR spectroscopy to detect the changes in extra virgin olive oil by adulteration with soybean oil and high temperature heat treatment, Open Chem. 13 (2015) 689, https://doi.org/10.1515/chem-2015-0110.
[86] SigmaAldrich, IR spectrum table by frequency range. https://www.sigmaaldrich.com/ES/en/technical-documents/technical-article/analytical-chemistry/photometry-and-reflectometry/ir-spectrum-table, 2024. (Accessed 22 January 2024).
[87] E. Dartois, G.M. Muñoz Caro, D. Deboffle, L. d'Hendecourt, Diffuse interstellar medium organic polymers, Astron. Astrophys. 423 (2004) L33, https://doi.org/10.1051/0004-6361:200400032.
[88] N. Vlachos, Y. Skopelitis, M. Psaroudaki, V. Konstantinidou, A. Chatzilazarou, E. Tegou, Applications of Fourier transform-infrared spectroscopy to edible oils, Anal. Chim. Acta 573–574 (2006) 459, https://doi.org/10.1016/j.aca.2006.05.034.
[89] NIST, NIST chemistry WebBook, NIST Standard Ref. Database Number 69 (2025). https://webbook.nist.gov/chemistry/. (Accessed 31 July 2025).
[90] M. Lozano, P. Rodríguez-Ulibarri, J.C. Echeverría, M. Beruete, M. Sorolla, M. J. Beriain, Mid-infrared spectroscopy (MIR) for simultaneous determination of fat and protein content in meat of several animal species, Food Anal. Methods 10 (2017) 3462, https://doi.org/10.1007/s12161-017-0879-1.
[91] L.M. Miller, M.W. Bourassa, R.J. Smith, FTIR spectroscopic imaging of protein aggregation in living cells, Biochim. Biophys. Acta, Biomembr. 1828 (2013) 2339, https://doi.org/10.1016/j.bbamem.2013.01.014.
[92] E.J.J. van Velzen, J.P.M. van Duynhoven, P. Pudney, P.L. Weegels, J.H. van der Maas, Factors associated with dough stickiness as sensed by attenuated total reflectance infrared spectroscopy, Cereal Chem. 80 (2003) 378, https://doi.org/10.1094/CCHEM.2003.80.4.378.